Biogeosciences Discuss., doi:10.5194/bg-2016-282, 2016
Manuscript under review for journal Biogeosciences
Published: 11 July 2016

Biogeosciences Discussions
Open Access
EGU

Manganese in the world ocean: a first global model

Marco van Hulten[1,6], Jean-Claude Dutay[1], Rob Middag[2,3,4], Hein de Baar[4,5], Matthieu Roy-Barman[1], Marion Gehlen[1], Alessandro Tagliabue[7], and Andreas Sterl[6]

[1]Laboratoire des Sciences du Climat et de l'Environnement (LSCE), IPSL, CEA–Orme des Merisiers, 91191 Gif-sur-Yvette, France
[2]University of Otago, 364 Leith Walk, Dunedin, 9016, New Zealand
[3]University of California Santa Cruz (UCSC), 1156 High Street, Santa Cruz, CA 95064, USA
[4]Royal Netherlands Institute for Sea Research (NIOZ), Landsdiep 4, 1797 SZ 't Horntje, Texel, the Netherlands
[5]University of Groningen (RUG), Postbus 72, 9700 AB Groningen, the Netherlands
[6]Royal Netherlands Meteorological Institute (KNMI), Utrechtseweg 297, 3731 GA De Bilt, the Netherlands
[7]University of Liverpool, 4 Brownlow Street, Liverpool L69 3GP, UK

Correspondence to: M. M. P. van Hulten (mvhulten@lsce.ipsl.fr)*

Abstract. Dissolved manganese (Mn) is a biologically essential element. Moreover, its oxidised form is involved in the removal of itself and several other trace elements from ocean waters. Recently, a large number of highly accurate Mn measurements has been obtained in the Atlantic, Indian and Arctic oceans as part of the GEOTRACES programme. The goal of this study is to combine these new observations with state-of-the-art modelling to give new insights into the main sources and redistribution of Mn throughout the ocean. To this end, we simulate the distribution of dissolved Mn using a global-scale circulation model. This first model includes simple parameterisations to account, realistically, for the sources, processes and sinks of Mn in the ocean. Whereas oxidation and (photo)reduction, as well as aggregation and settling are parameterised in the model, biological uptake is not yet taken into account by the model. Our model reproduces observations accurately and provides the following insights:

- The high surface concentrations of manganese are caused by the combination of photoreduction and sources to the upper ocean. The most important sources are dust, then sediments, and, more locally, rivers.
- Results show that surface Mn in the Atlantic Ocean moves downwards into the North Atlantic Deep Water, but because of strong removal rates the Mn does not propagate southwards.
- There is a mainly homogeneous background concentration of dissolved Mn of about $0.10\ \mathrm{nM}$ to $0.15\ \mathrm{nM}$ throughout most of the deep ocean. The model reproduces this by means of a threshold on particulate manganese oxides of $25\ \mathrm{pM}$, suggesting that a minimal concentration of particulate Mn is needed before aggregation and removal become efficient.
- The observed sharp hydrothermal signals are produced by assuming both a high source and a strong removal of Mn near hydrothermal vents.

*Postprints may be found at arXiv:1606.07128.

Biogeosciences Discuss., doi:10.5194/bg-2016-282, 2016
Manuscript under review for journal Biogeosciences
Published: 11 July 2016

Biogeosciences Discussions Open Access EGU

1 Introduction

Dissolved manganese ($\mathrm{Mn_{diss}}$) is taken up by phytoplankton, because Mn is crucial for photosynthesis and other biological functions (Raven, 1990). Furthermore, its oxidised form ($\mathrm{Mn_{ox}}$) plays an important role in the removal of several other trace metals from seawater (Yamagata and Iwashima, 1963). While in the open ocean manganese (Mn) exists in small concentrations, it is the twelfth most plentiful element in the Earth's crust (Wedepohl, 1995). Seawater Mn occurs in many forms, among which the bioavailable dissolved form which is available for incorporation in organisms and marine particles. After phytoplankton death, incorporated Mn sinks downwards together with the dead material, but most of the organic material remineralises before reaching the sea floor (Sarmiento and Gruber, 2006).

Another important mechanism of storing Mn in particles, besides biological incorporation, is the removal of dissolved Mn(II) via colloids on which the Mn is oxidised to insoluble Mn(IV) (and possibly other oxidation states), and the subsequent aggregation by particulate matter. Oxidation occurs everywhere in the ocean where oxygen is available. This process may be strongly accelerated by Mn(II)-oxidising microorganisms, primarily bacteria and fungi (Sunda and Huntsman, 1988, 1994; Tebo et al., 2005), but we do not understand the role of these organisms quite well (Nealson, 2006).

The reverse process is the reduction of Mn oxides to bioavailable dissolved Mn(II), i.e. $\mathrm{Mn^{2+}}$. The full oxidation/reduction (redox) equilibrium reaction, in its most simple form, is given by (Froelich et al., 1979):

$$\mathrm{Mn^{2+} + \frac{1}{2}\,O_2 + H_2O \quad \rightleftharpoons \quad MnO_2 + 2\,H^+}\ ,$$

where oxidation is towards the right and reduction towards the left. Reduction is significantly faster under the influence of sunlight. It is hence referred to as *photoreduction* when irradiance is the major contributor. This process, together with the atmospheric source, is responsible for the high $\mathrm{Mn_{diss}}$ concentration in the euphotic zone. The relative speed of photoreduction compared to oxidation is important for Mn(II) availability. An overall net higher oxidation rate implies more scavenging, hence more Mn export.

Manganese enters the open ocean through lithogenic dust deposition (Baker et al., in preparation) and lateral advection from reducing sediments (Homoky et al., in preparation). Surface [$\mathrm{Mn_{diss}}$] is especially high in the central Atlantic Ocean and up to at least 30° N because of high dust input from the Sahara in combination with photoreduction (Landing and Bruland, 1987; Jickells, 1995; Guieu et al., 1994; Baker et al., 2006; De Jong et al., 2007; Wu et al., 2014). Similarly, [$\mathrm{Mn_{diss}}$] is high in the northern Indian Ocean (Thi Dieu Vu and Sohrin, 2013). Dissolved Mn diffuses out of anoxic sediments, because sediment microorganisms reduce $\mathrm{Mn_{ox}}$ if there is no more oxygen (or nitrate) left (Li et al., 1969; Landing and Bruland, 1980; Sundby and Silverberg, 1985; Pakhomova et al., 2007; Middag et al., 2012; Sarmiento and Gruber, 2006, p. 234). Rivers are another source of Mn to the ocean (Elderfield, 1976; Aguilar-Islas and Bruland, 2006). While much of the fluvial Mn sediments by scavenging and aggregation, a large part may finally be transported to the ocean by diffusion from and resuspension of the sediments (Jeandel, in preparation; Charette et al., in preparation). Typically, the smaller sediment particles (0.5 µm to 4 µm) contain a lot of manganese, and, because of their small size, are able to reach the open ocean (Yeats et al., 1979; Sundby et al., 1981; Trefry and Presley, 1982). Manganese may also flux into the ocean by melting sea ice (Middag et al., 2011b). Finally,

Biogeosciences Discuss., doi:10.5194/bg-2016-282, 2016
Manuscript under review for journal Biogeosciences
Published: 11 July 2016

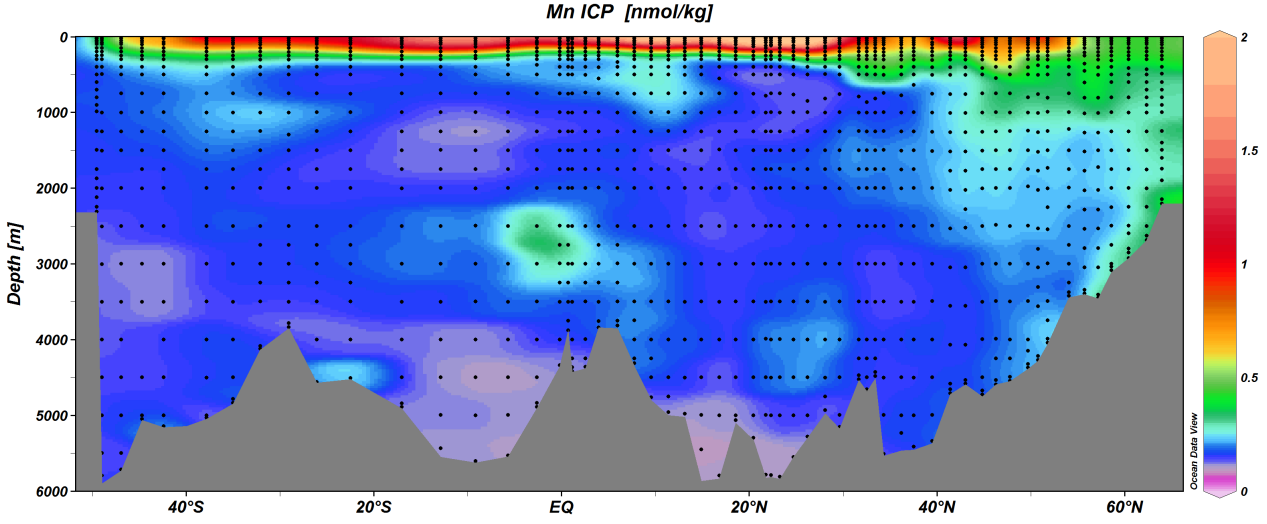

Figure 1. Observations of $[\mathrm{Mn_{diss}}]$ (nM) along the GEOTRACES GA02 transect in the West Atlantic Ocean. Dots are the locations of the measurements. Appendix A contains sampling and analysis methods performed along this transect.

overwhelming evidence is found of manganese fluxing out of hydrothermal vents (Klinkhammer et al., 1977, 1985; Hydes et al., 1986; Klinkhammer et al., 2001; Middag et al., 2011b, a; German et al., in preparation).

Downward fluxes of settling particles that have been collected in sediment traps show a strong correlation between lithogenic particles and Mn (Roy-Barman et al., 2005). Therefore lithogenic particles are likely to play a significant role in the removal (oxidation, scavenging and aggregation) of Mn. Here the ballast effect of lithogenic particles, which typically have a density of about twice of that of seawater, is likely playing a major role for rapid settling of agglomerates of biogenic and lithogenic particles including Mn-oxides coatings Balistrieri et al. (1981). This is consistent with the fact that most particles are small (less than 2 µm), but larger aggregates are significant contributors to the vertical flux (McCave, 1975; Bishop and Fleisher, 1987). The complete process may be more complicated than described above (Boyle et al., 2005), e.g. because Mn possibly binds to ligands such that it stays in solution (Sander and Koschinsky, 2011; Madison et al., 2013).

Manganese oxides are important scavengers of other trace metals like iron, cobalt, nickel and zinc (Yamagata and Iwashima, 1963; Murray, 1975; Means et al., 1978; Saito et al., 2004; Tonkin et al., 2004), as well as insoluble radionuclides such as thorium and protactinium (e.g Reid et al., 1979; Hayes et al., 2015; Jeandel et al., 2015). Therefore, Mn availability does not only directly impact primary production but may also play a role in removing other elements from the surface ocean. These elements include biologically essential trace metals as well as many more trace elements.

Figure 1 shows the West Atlantic GEOTRACES transect. The concentration of $\mathrm{Mn_{diss}}$ near the ocean surface is high, and its distribution is mainly homogeneous in the intermediate and deep ocean. The only prominent deviations from the "background" $[\mathrm{Mn_{diss}}] \approx 0.15\ \mathrm{nM}$ in the subsurface ocean are the elevated values near the Mid-Atlantic Ridge. What makes the distribution

Biogeosciences Discuss., doi:10.5194/bg-2016-282, 2016
Manuscript under review for journal Biogeosciences
Published: 11 July 2016

of $\mathrm{Mn_{diss}}$ so relatively homogeneous in the interior of the ocean, except for a few localised features where $[\mathrm{Mn_{diss}}]$ is notably elevated? The elevated local features are located at around $2.5\ \mathrm{km}$ depth on the Zero Meridian at 50° S (presented on Fig. 6) as well as the West Atlantic Ocean at, and just south of, the equator, and at the Denmark Strait overflow (Fig. 1). The elevations of $[\mathrm{Mn_{diss}}]$ in the Southern Hemisphere can be ascribed to hydrothermal activity near those regions. The sources north of 40° N may be supplied by mixing high $[\mathrm{Mn_{diss}}]$ surface waters downwards, but other sources may be (partly) responsible as well, among which diffusive sediments and hydrothermal vents. Dust deposition and photoreduction explain the high $[\mathrm{Mn_{diss}}]$ at the surface, especially under and downstream of dust deposition sites. This leaves the question of the non-zero homogeneous $\mathrm{Mn_{diss}}$ "background distribution" in the rest of the ocean. In this study, we will test a simple mechanism that should be able to give insight into this stable $\mathrm{Mn_{diss}}$ concentration.

Until now only local model simulations of the Mn ocean cycle have been performed that focus on the processes most relevant for the respective regions. The case of hydrothermal activity has been studied by Lavelle et al. (1992) who modelled Mn in the deep ocean near hydrothermal vents. They included four Mn tracers, namely, a dissolved form, small particles associated with bacteria, larger aggregate particles, and one in sediments as the model includes benthic fluxes. They found that "more than 80 % of the hydrothermal Mn is deposited within several hundred kilometres of the ridge crest though dissolved Mn concentrations beyond that distance exceed background levels by many times". This illustrates both the high Mn input from hydrothermal vents and the high removal rate.

The $\mathrm{Mn_{diss}}$ distribution in the North Pacific Ocean has been modelled by Johnson et al. (1996), in a 1-D vertical model neglecting horizontal transport. Their oxidation model depends on $[\mathrm{O_2}]$ and $\{\mathrm{OH^-}\}$. Their region of interest was on the upper and intermediate depth ocean, and their goal was to reproduce the $[\mathrm{Mn_{diss}}]$ maximum in the Oxygen Minimum Zone (OMZ). Except for the North Pacific, the OMZ is also present in other basins, amongst which the northwestern Indian Ocean (Saager et al., 1989; Lewis and Luther, 2000). Johnson et al. (1996) found that the combination of remineralisation rates and decreased oxidation in the OMZ explained their $[\mathrm{Mn_{diss}}]$ profiles. In the euphotic zone $\mathrm{Mn_{diss}}$ was incorporated in phytoplankton, while remineralised $\mathrm{Mn_{diss}}$ in the aphotic (and disphotic) zone was lost by oxidation and scavenging.

While these modelling efforts are useful for their purposes, no studies exist in which the global ocean $\mathrm{Mn_{diss}}$ distribution is modelled. To arrive at a more integrated understanding of the oceanic Mn cycle, we include a Mn model in an ocean general circulation model. This is the first time that a global ocean model for manganese has been written and assessed. It is a basic model that should give a starting point for other studies. While there is of course uptake of Mn by phytoplankton, and sometimes it is even a limiting element (Middag et al., 2013), we do not include biology in the model. The reason is that at the moment there is no clear evidence for typical uptake-remineralisation processes as is the case for, e.g., iron. While we perform a model simulation on a global scale, we give more attention to the $\mathrm{Mn_{diss}}$ distribution in the Atlantic Ocean. Specifically, two dense and high-accuracy datasets as part of the GEOTRACES programme were available at the time of this study, namely the GA02 in the West Atlantic and the GIPY5 at the Zero Meridian in the Southern Ocean (Middag et al., 2011a, in preparation). Furthermore, in those regions we can study potentially important properties of the ocean geochemistry of manganese and the interaction with circulation, among which the Atlantic overturning circulation and hydrothermal activity.

Biogeosciences Discuss., doi:10.5194/bg-2016-282, 2016
Manuscript under review for journal Biogeosciences
Published: 11 July 2016

In this study our goal is to assess the fundamental processes that are the most important to realistically simulate [$\mathrm{Mn_{diss}}$], including the aforementioned properties of the dissolved Mn distribution. To this end, we will first introduce our Mn model with its processes, sources and sinks. We will show the results of a realistic reference simulation, which will be compared with recent high-accuracy observations. Also two sensitivity simulations will be presented, studying the effects of the intense nature of hydrothermal vents and a strong Mn removal that depends on specific conditions.

2 Methods

2.1 Model dynamics and configuration

In order to simulate the three-dimensional (3-D) distribution of dissolved Mn, we use the general circulation model *Océan PArallélisé* (OPA) (Madec et al., 1998) that is part of NEMO, a framework for ocean models (Madec, 2008). We use the ORCA2-LIM configuration of NEMO. The spatial resolution is about 2° by 2° $\cos(\phi)$ (where ϕ is the latitude) with an increased meridional resolution to 0.5° in the equatorial domain. The model has 30 vertical layers, with an increased vertical thickness from $10\ \mathrm{m}$ at the surface to $500\ \mathrm{m}$ at $5000\ \mathrm{m}$ depth. Representation of the topography is based on the partial-step thickness (Barnier et al., 2006). Lateral mixing along isopycnal surfaces is performed both on tracers and momentum (Lengaigne et al., 2003). The parameterisation of Gent and McWilliams (1990) is applied from 10° poleward to represent the effects of non-resolved mesoscale eddies. Vertical mixing is modelled using the turbulent kinetic energy (TKE) scheme of Gaspar et al. (1990), as modified by Madec (2008). The fluid dynamics used to drive our model is identical to that used in Aumont et al. (2015).

2.2 Manganese model

There are two tracers of Mn, referred to as dissolved ($\mathrm{Mn_{diss}}$) and oxidised ($\mathrm{Mn_{ox}}$) manganese. The dissolved phase is operationally defined, and may contain phases different from Mn(II). These tracers are driven by the equations set out in this section, as well as the velocity fields obtained from OPA, the dynamical component of NEMO. Instead of calculating the dynamical variables of the model (velocity and mixing), we run it off-line, using a five-daily climatology.

Figure 2 presents the conceptual scheme of our manganese model. The internal processes are oxidation, reduction, aggregation and burial (blue arrows in the figure). Rivers, dust, sediments and hydrothermal vents are presented as arrows at the top and bottom of the figure. These four Mn sources are presented in Fig. 3, and Table 1 lists the absolute contributions to the different basins by each of these sources, as well as the relative contribution of every source to the world ocean.

In the following subsections we will describe how the different sources and processes are included in the model. The model parameters are summarised in Table 2.

Biogeosciences Discuss., doi:10.5194/bg-2016-282, 2016
Manuscript under review for journal Biogeosciences
Published: 11 July 2016

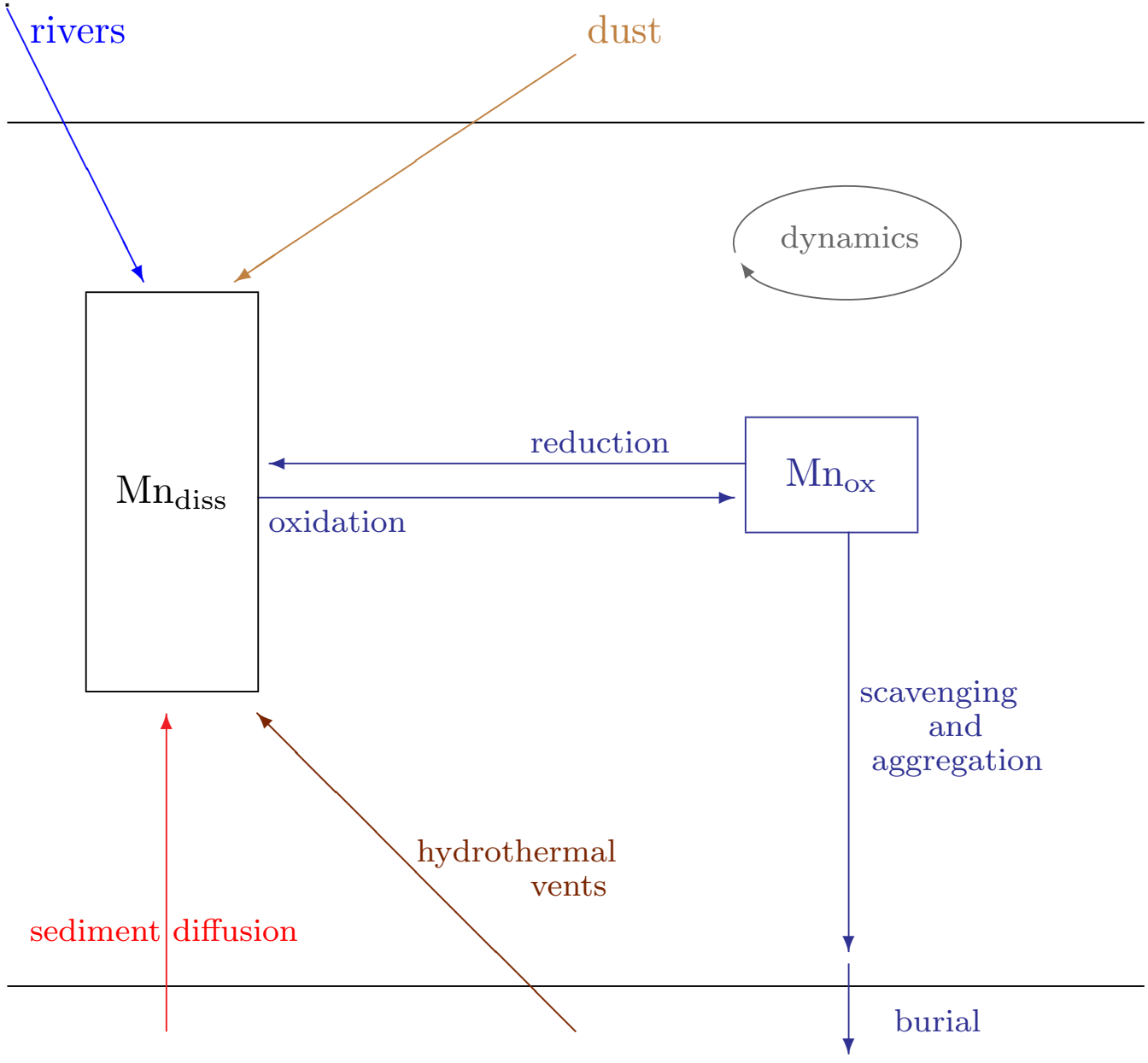

Figure 2. Model scheme. Redox and scavenging are in blue; circulation and mixing (dynamics) in grey; and the sources dust, rivers, hydrothermal and sediment are in light brown, light blue, dark brown and red, respectively. Mn_{diss} is the dissolved and Mn_{ox} the oxidised Mn.

Biogeosciences Discuss., doi:10.5194/bg-2016-282, 2016
Manuscript under review for journal Biogeosciences
Published: 11 July 2016

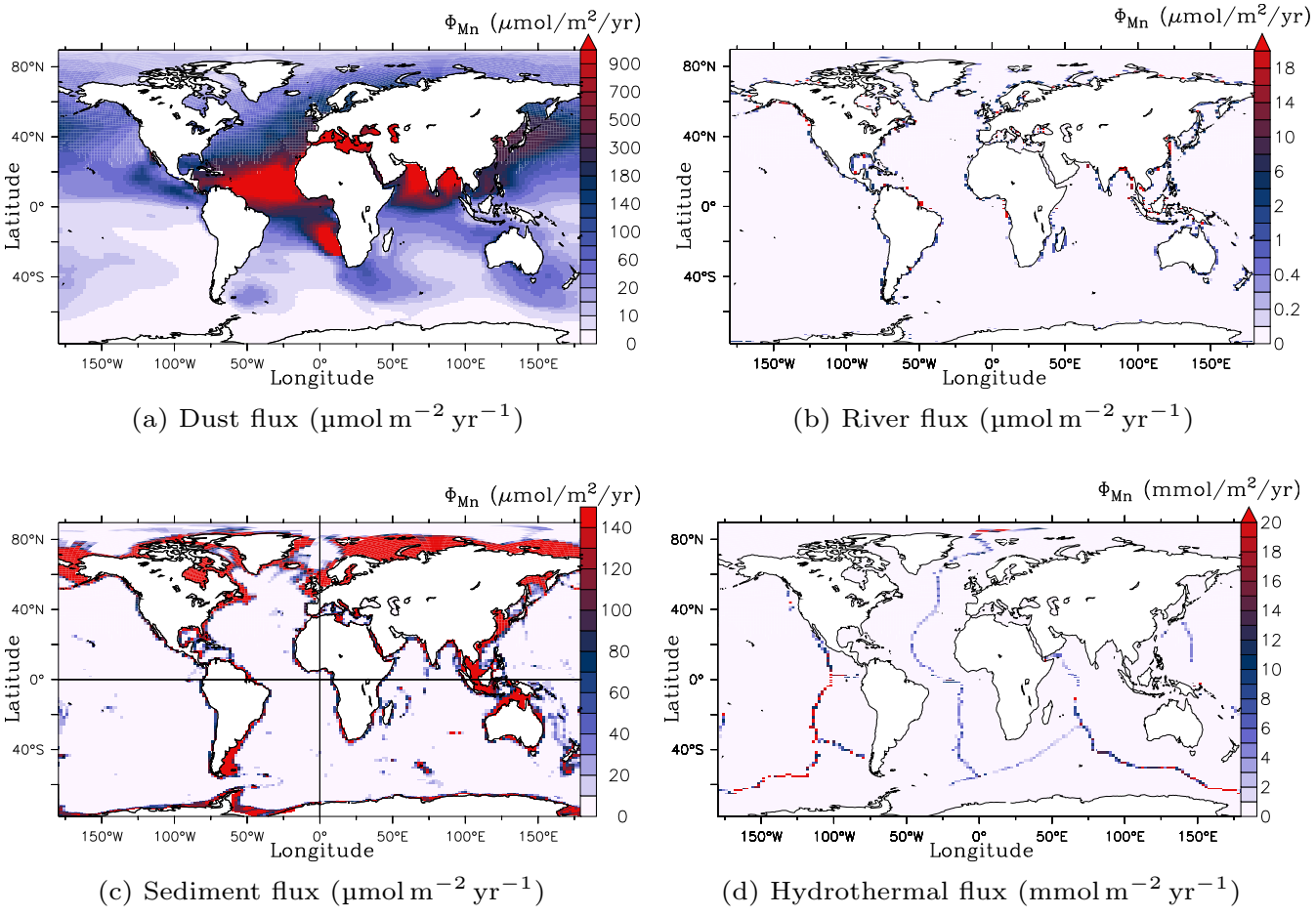

Figure 3. Sources of Mn to the ocean: effective $\mathrm{Mn_{diss}}$ input flux Φ. Three-dimensional fields are vertically integrated, such that dimensions are molar fluxes. Ranges vary between the different sources.

2.2.1 Atmospheric dust source

Manganese is added to the pool of $\mathrm{Mn_{diss}}$ in the upper model layer, according to

$$\left.\frac{\partial \mathcal{D}}{\partial t}\right|_{\mathrm{dust}} = \frac{\alpha \cdot f_{\mathrm{Mn,dust}}}{m \cdot \Delta z_1} \cdot \Phi_{\mathrm{dust}}\,, \tag{1}$$

where $\mathcal{D}$ is the dissolved Mn concentration, α is the solubility of Mn in dust, $f_{\mathrm{Mn,dust}}$ is the mass fraction of Mn in dust, m is the molar mass of Mn, $\Delta z_1 = 10\,\mathrm{m}$ is the upper model layer thickness. The lithogenic dust deposition flux, Φ_{dust}, is derived from the Interaction with Chemistry and Aerosols (INCA) model (Hauglustaine et al., 2004). Here we use a $12\,\mathrm{mo}$ climatology of INCA's output as a forcing.

The average mass fraction of Mn in the Earth's upper crust is 527 ppm (Wedepohl, 1995). However, the fraction measured in Saharan dust is 880 ppm (Mendez et al., 2010), consistent with Guieu et al. (1994) and Statham et al. (1998). Since most of

Biogeosciences Discuss., doi:10.5194/bg-2016-282, 2016
Manuscript under review for journal Biogeosciences
Published: 11 July 2016

Basin	Dust	Rivers	Sediment	Hydrothermal
Atlantic Ocean	29355	46	1848	13760
Pacific Ocean	8714	39	2475	60146
Indian Ocean	9829	39	883	22483
Southern Ocean	58	0	413	7601
Arctic Ocean	405	8	926	2269
Mediterranean Sea	3756	115	183	0
total amount ($\mathrm{Mmol\,yr^{-1}}$)	52117	137	6727	106259
relative amount (%)	31.5	0.1	4.1	64.3

Table 1. Absolute amount of effective annual input of Mn by means of sediment, river and hydrothermal input into each basin ($\mathrm{Mmol\,yr^{-1}}$). The Southern Ocean is defined as the ocean south of 58.7° S. The line "total amount" denotes how much world-wide Mn is added to the ocean due to a specific flux; "relative amount" is normalised to the total Mn input flux.

Parameter	Symbol	Value used	Known range	References
Mass fraction of Mn in dust	$f_{\mathrm{Mn,dust}}$	880 ppm	696 to 880 ppm	Wedepohl (1995); Mendez et al. (2010)
Dust Mn solubility	α	30 %	10 to 70 %	Baker et al. (2006)
Sediment source Mn/Fe ratio	$r_{\mathrm{Mn:Fe,sed}}$	0.2	uncertain	Bortleson and Lee (1974); Slomp et al. (1997)
River source Mn/Fe ratio	$r_{\mathrm{Mn:Fe,riv}}$	0.214	uncertain	Sarmiento and Gruber (2006, p. 2)
Hydrothermal Mn/^{3}He ratio	$r_{\mathrm{Mn:^3He,hydro}}$	0.10×10^9	uncertain	-
Settling speed of $\mathrm{Mn_{ox}}$	w_{ox}	1–10 $\mathrm{m\,d^{-1}}$	0.9–1.4 $\mathrm{m\,d^{-1}}$	Roy-Barman (2009)
Oxidation rate constant	k_{ox}	0.341×10^{-3} $\mathrm{h^{-1}}$	uncertain	Bruland et al. (1994)
Photoreduction rate constant	$k_{\mathrm{red,light}}$	98×10^{-3} $\mathrm{h^{-1}}$	$50–150 \times 10^{-3}$ $\mathrm{h^{-1}}$	Sunda and Huntsman (1994)
Aphotic reduction rate	$k_{\mathrm{red,dark}}$	1.70×10^{-3} $\mathrm{h^{-1}}$	$0.98–14.3 \times 10^{-3}$ $\mathrm{h^{-1}}$	Bruland et al. (1994)
Aggregation threshold	$\mathcal{X}_{\mathrm{thr}}$	25 pM	hypothetical	-

Table 2. Mn model parameters for the *Reference* simulation. The settling velocity w_{ox} is given by Eq. 11. In *LowHydro* the hydrothermal flux and the maximum settling speed are both reduced by a factor of 10 ($r_{\mathrm{Mn:^3He,hydro}} = 0.01 \times 10^9$; and $w_{\mathrm{ox}} \equiv 1\,\mathrm{m\,d^{-1}}$ or, equivalently, $\mathcal{X}_{\mathrm{thr}} \to \infty$). In the sensitivity simulation *NoThreshold* the aggregation threshold $\mathcal{X}_{\mathrm{thr}}$ is set to zero.

the dust deposited on the Atlantic Ocean originates from the Sahara and our focus is the Atlantic Ocean, the value of 880 ppm is used for $f_{\mathrm{Mn,dust}}$.

The solubility of Mn from dust is uncertain and relatively high compared to most other trace metals. Here $\alpha = 30\,\%$ of the Mn in dust is assumed to dissolve, largely consistent with the values reported by Guieu et al. (1994); Jickells (1995); Baker

Biogeosciences Discuss., doi:10.5194/bg-2016-282, 2016
Manuscript under review for journal Biogeosciences
Published: 11 July 2016

et al. (2006); De Jong et al. (2007); Buck et al. (2010). Several studies report even higher values ($> 50\,\%$), which are, however, mainly from anthropogenic or otherwise processed dust, while the lower reported values ($< 50\,\%$) are from natural dust, mainly of Saharan origin.

Figure 3a presents the average Mn dissolution flux of the $12\ \mathrm{mo}$ climatology.

2.2.2 River source

The manganese river source is modelled analogously to iron, which is part of the biogeochemical model PISCES (Aumont et al., 2015). This means that our manganese influx is proportional to the total dissolved (organic and inorganic) carbon flux, just like for iron (Aumont et al., 2015). Hence, the modelled concentration change of $\mathrm{Mn_{diss}}$ caused by river input is given by

$$\left.\frac{\partial \mathcal{D}}{\partial t}\right|_{\text{rivers}} = r_{\text{Mn:Fe,river}} \cdot \left.\frac{\partial [\mathrm{Fe_{diss}}]}{\partial t}\right|_{\text{rivers}}, \tag{2}$$

where $[\mathrm{Fe_{diss}}]$ is the dissolved iron concentration, and $r_{\text{Mn:Fe,river}}$ is the effective manganese/iron flux ratio, here set to 0.214, based on river dissolved concentrations (Sarmiento and Gruber, 2006, p. 2). For comparison, it is much higher than the crustal ratio, which is around 0.02 (Wedepohl, 1995), but probably underestimated as we do not consider external sources of particulate manganese. The effective $\mathrm{Mn_{diss}}$ input into the ocean by rivers is presented in Fig. 3b.

2.2.3 Sediment source

The largest contribution of Mn to the upper ocean is dust deposition, but over large shelf and slope regions (e.g. polar oceans) the flux of $\mathrm{Mn_{diss}}$ from the sediment can be of the same order of magnitude as the dust deposition flux (e.g. Middag et al., 2013, for the Southern Ocean).

As long as there is oxygen in the sediment, the organic carbon is remineralised by using this oxygen as an electron acceptor. This process produces $\mathrm{CO_2}$ that fluxes out of the sediments. As soon as oxygen is mostly depleted, nitrate is used as an oxidiser, producing both $\mathrm{N_2}$ and $\mathrm{CO_2}$; this is called denitrification. Around the same time, Mn reduction takes place, converting $\mathrm{MnO_2}$ to dissolved $\mathrm{Mn(II)}$ that fluxes out of the sediment into bottom waters (Pakhomova et al., 2007; Middag et al., 2011a). After that iron reduction takes over as the primary redox reaction. Oxygen oxidation has the most negative free energy change, then manganese and nitrate (depending on the $\mathrm{MnO_2}$ phase being reduced), and so on; this determines the order of reactions (Froelich et al., 1979).

The (redox) reactions in the sediment are not explicitly modelled, since the sediment is not part of our model domain. Therefore, Mn addition from the sediment is modelled as a prescribed source. Since we do not have global maps of $\mathrm{Mn_{diss}}$ sediment–seawater flux, we parameterise the flux based on existing parameterisations of nitrate and iron.

Middelburg et al. (1996) derived an empirical model for calculating the denitrification rate as a function of the seafloor depth:

$$\zeta_{\text{Fsed}} = -0.9543 + 0.7662 \cdot \ln(z_{\text{Fsed}}) - 0.235 \cdot \ln(z_{\text{Fsed}})^2\,. \tag{3}$$

Biogeosciences Discuss., doi:10.5194/bg-2016-282, 2016
Manuscript under review for journal Biogeosciences
Published: 11 July 2016

Aumont et al. (2015) used this model for their sediment source of dissolved Fe in the PISCES model. They used a high-resolution bathymetric map to account for the shallow shelves, and modulated the seafloor depth ($z \rightarrow z_{\text{Fsed}}$) as follows:

$$z_{\text{Fsed}} = \min\left(8, \left(\frac{z}{500\,\text{m}}\right)^{-1.5}\right). \tag{4}$$

They set the maximum iron flux to $2\,\mu\text{mol}\,\text{m}^{-2}\,\text{s}^{-1}$. Assuming a porewater ratio $r_{\text{Mn:Fe,sed}} = 0.2$, and following the same method as Aumont et al. (2015), our final sediment addition of Mn_{diss} into bottom water is given by:

$$\left.\frac{\partial \mathcal{D}}{\partial t}\right|_{\text{sediments}} = \frac{0.4\,\mu\text{mol}\,\text{m}^{-2}\,\text{s}^{-1}}{\Delta z_{\text{sed}}} \cdot \min(1,\, 2\text{e}^{\zeta_{\text{Fsed}}}), \tag{5}$$

where z_{sed} is the gridbox thickness of the bottom gridbox (just above the seafloor). With this prescribed source, the Mn flux is limited to a maximum of about $150\,\mu\text{mol}\,\text{m}^{-2}\,\text{yr}^{-1}$. This can be seen in Fig. 3c: the higher-than-$140\,\mu\text{mol}\,\text{m}^{-2}\,\text{yr}^{-1}$ regions on the shelves is especially notable as it falls in the upper (red) part of the colour scale.

2.2.4 Hydrothermal source

Hydrothermal vent Mn_{diss} fluxes are modelled proportional to that of ^3He in Rüth et al. (2000) and Dutay et al. (2004). This approach is shown to have worked for iron (Bowers et al., 1988; Douville et al., 2002; Tagliabue et al., 2010; Resing et al., 2015). The basic equation for the change of Mn_{diss} from hydrothermal vent influx is

$$\left.\frac{\partial \mathcal{D}}{\partial t}\right|_{\text{hydrothermal}} = r_{\text{Mn:}^3\text{He,hydro}} \cdot \frac{\partial[^3\text{He}]}{\partial t}, \tag{6}$$

where $r_{\text{Mn :}^3\text{ He,hydro}} = 0.1 \times 10^9$ is the ratio between the Mn_{diss} and ^3He effective inflow from hydrothermal vents into the model domain. Recent observational studies found $\text{Mn}_{\text{diss}}/^3\text{He}$ concentration ratios of 4.0×10^6 (Kawagucci et al., 2008) and 3.5×10^6 (Resing et al., 2015) very close to hydrothermal outflux regions. To satisfy this, we assume that a dissolved fraction of 4 % is left when the hydrothermal plume reaches the observational sites.

This high "solubility fraction" means that the hydrothermal vents are a large source of Mn_{diss} compared to Fe (Tagliabue et al., 2010; Resing et al., 2015). In our simulations we will show that such a large flux is necessary. This choice also relates to the fast modelled removal rate of Mn near the depth of hydrothermal vents (explained later). The hydrothermal Mn_{diss} source is presented in Fig. 3d.

2.2.5 Redox processes

Reduction and oxidation of Mn within the water column is a combination of several processes. Firstly, Mn_{ox} is subject to non-biological reduction, significantly stimulated by sunlight (e.g. Sunda and Huntsman, 1994). Secondly, the rate of oxidation is enhanced by microbes (bacteria and fungi) in regions where Mn_{diss} supply is high (Sunda and Huntsman, 1994; Tebo et al., 2005), and it depends on the O_2 concentration and pH. This has been observed in the North Pacific Ocean (Johnson et al., 1996, and references therein), as well as in some GEOTRACES transects in the Atlantic Ocean. However, measurements from the West Atlantic Ocean and Zero-Meridian Southern Ocean GEOTRACES cruises do not show a clear minimum of $[\text{Mn}_{\text{diss}}]$

Biogeosciences Discuss., doi:10.5194/bg-2016-282, 2016
Manuscript under review for journal Biogeosciences
Published: 11 July 2016

between the euphotic and oxygen minimum zones. At this stage we decide to not include a dependency on $[O_2]$ to the model. Hence, here we choose to model Mn following a pseudo-first-order reaction where k_{ox} and k_{red} are pseudo-first-order rate constants (conventional primes omitted, e.g. Stone and Morgan, 1990):

$$\frac{\partial \mathcal{D}}{\partial t}\Big|_{redox} = -k_{ox}\mathcal{D} + k_{red}\mathcal{X} \tag{7}$$

$$\frac{\partial \mathcal{X}}{\partial t}\Big|_{redox} = k_{ox}\mathcal{D} - k_{red}\mathcal{X}\,, \tag{8}$$

where $\mathcal{X}$ is the particulate oxidised Mn concentration, and

$$k_{red} = \begin{cases} k_{red,light} & \text{in the euphotic zone} \\ k_{red,dark} & \text{elsewhere}\,, \end{cases} \tag{9}$$

with $k_{red,light} \gg k_{red,dark}$, since reduction is much stimulated by sunlight (Table 2). The euphotic zone is defined as the depths where the sunlight penetration is at least 1 %.

2.2.6 Settling and burial

Manganese oxides settle, resulting in a concentration change according to

$$\frac{\partial \mathcal{X}}{\partial t}\Big|_{settling} = -w_{ox} \cdot \frac{\partial \mathcal{X}}{\partial z}\,, \tag{10}$$

where w_{ox} is the settling velocity, set to a constant $1\ \mathrm{m\,d^{-1}}$ as long as $[Mn_{ox}] \leq 25\ \mathrm{pM}$. The manganese oxide is buried when arriving at the ocean floor, which means that it is removed from the model domain. If $[Mn_{ox}] > 25\ \mathrm{pM}$, the settling velocity is not a constant any more but a function of depth. Still, in the mixed layer $w_{ox} = 1\ \mathrm{m\,d^{-1}}$, but if $[Mn_{ox}] > 25\ \mathrm{pM}$ the sinking speed increases linearly up to its maximum of $10\ \mathrm{m\,d^{-1}}$ at $2.5\ \mathrm{km}$ depth.

The rationale for increasing the settling velocity above a certain threshold is that if Mn_{ox} is large enough, dense aggregates form that have faster sinking rates. Notably mineral particles (sand, clay, carbonate) of high density in the order of 2–3 times that of seawater are responsible for this (McCave, 1975). Particulate organic carbon may play an important role as well (Passow and De La Rocha, 2006). In this way, $[Mn_{diss}]$ keeps in check while still providing a deep ocean sink. As long as this critical particulate Mn concentration of $25\ \mathrm{pM}$ is not reached, aggregation of small Mn_{ox} particles does not yet occur. The choice of the critical concentration of $25\ \mathrm{pM}$, also referred to as the *aggregation threshold*, is derived from the redox rate constants in combination with a typical, low value of the observed dissolved Mn concentration (here chosen as $0.125\ \mu\mathrm{M}$): $\mathcal{X}_{thr} = (k_{ox}/k_{red,dark}) \cdot 0.125\ \mu\mathrm{M} = 25\ \mathrm{pM}$. More precisely, settling of Mn_{ox} follows Eq. (10) with the settling velocity

$$w_{ox}/(\mathrm{m\,d^{-1}}) = 1 + 9 \cdot \max\left(0, \frac{z - MLD}{2.5\ \mathrm{km}}\right) \cdot H(\mathcal{X} - \mathcal{X}_{thr})\,, \tag{11}$$

where z is the depth, *MLD* is the mixed layer depth, H the Heaviside step function, and $\mathcal{X}_{thr}$ is the aggregation threshold set to $25\ \mathrm{pM}$.

The source code of the manganese model is attached to this publication as a Supplement.

Biogeosciences Discuss., doi:10.5194/bg-2016-282, 2016
Manuscript under review for journal Biogeosciences
Published: 11 July 2016

Simulation name	$r_{\mathrm{Mn:^3He,hydro}}$	$w_{\mathrm{ox}}(\mathrm{m\,d^{-1}})$	$\mathcal{X}_{\mathrm{thr}}$
Reference	0.10×10^9	1–10	25 pM
LowHydro	$\mathbf{0.01 \times 10^9}$	**1**	–
NoThreshold	0.10×10^9	1–10	**0**

Table 3. List of simulations with the parameters changed compared to the reference simulation in boldface.

2.3 Simulations

The base simulation, *Reference*, was spun up for 500 yr to reach a steady state. *Reference* uses the parameters listed in Table 2. From year 100 onwards two sensitivity simulations were forked off to run in parallel with *Reference* for another 400 yr. These simulations are variations of the reference simulation. Table 3 lists the simulations and key parameters.

The simulation *LowHydro* is intended to test if the high $\mathrm{Mn_{diss}}$ input from hydrothermal vents is necessary or realistic. We first decreased the settling velocity to a constant $1\ \mathrm{m\,d^{-1}}$ (or, equivalently, $\mathcal{X}_{\mathrm{thr}} \to \infty$), which, as expected, resulted in a wide spreading of $\mathrm{Mn_{diss}}$ and a too high $[\mathrm{Mn_{diss}}]$ almost everywhere in the deep ocean (not presented). Then we decreased the hydrothermal flux by a factor of 10 to see whether the concentration of $\mathrm{Mn_{diss}}$ would become reasonable again without removing the hydrothermal plume signal. Thus *LowHydro* contains two changes compared to the *Reference* simulation: a tenfold decrease in both the hydrothermal flux and the maximum settling velocity.

In our third and final simulation, *NoThreshold*, we want to see if an aggregation threshold is needed for a realistic $[\mathrm{Mn_{diss}}]$ simulation. The threshold is removed by setting $\mathcal{X}_{\mathrm{thr}}$ to zero.

2.4 Observations

In this study we will mainly use data from the GEOTRACES programme, but for a worldwide global ocean comparison one has to rely also on data that were collected in the era before the reference samples of SAFe and GEOTRACES were available. Table 4 lists the datasets from GEOTRACES expeditions, as well as several other datasets; Fig. 4 shows the coordinates of the stations.

These observations are used for a visual global ocean data-model comparison (see appendix for method). Details on the statistical and visual model–data comparison are presented in Appendix B. Of these observations, only the West Atlantic Ocean data (the GEOTRACES GA02 transect, consisting of 64 PE 319, PE 321 and JC057; 1440 points) and the Zero-Meridian Southern Ocean data (GIPY4; 570 points) have been used for statistical comparison with the model. Moreover, only the data of the shipboard Flow Injection Analysis (FIA) have been used, which have five stations less than the on-shore mass spectrometry determinations. Both methods have advantages and disadvantages, but the results are almost identical (Middag, 2010). The measurements in the West Atlantic Ocean and polar oceans have a high accuracy and precision, as further described in the appendix. The focus of this study is the West Atlantic Ocean for several reasons. Firstly, recently measurements have been carried out in that region, resulting in a large consistent (one method) dataset. Other regions generally contain fewer measure-

Biogeosciences Discuss., doi:10.5194/bg-2016-282, 2016
Manuscript under review for journal Biogeosciences
Published: 11 July 2016

Transect	Year	Expedition	Ocean basin	Citation	#
GEOTRACES transects					
GIPY11	2007	ARK XXII/2	Arctic Ocean	Middag et al. (2011b)	773
GIPY4	2008	MD166 BONUS-GoodHope	Southern Ocean	Boye et al. (2012)	233
GIPY5	2008	ANT XXIV/3	Southern Ocean		
			a) Zero Meridian	Middag et al. (2011a)	468
			b) Weddell Sea	Middag et al. (2013)	176
			c) Drake Passage	Middag et al. (2012)	221
GI04	2009/2010	KH-09-5	Indian Ocean	Thi Dieu Vu and Sohrin (2013)	233
GA02	2010	64 PE 319	Northwest Atlantic Ocean	Middag et al. (in preparation)	384
GA02	2010	64 PE 321	Northwest Atlantic Ocean	Middag et al. (in preparation)	504
GA02	2011	JC057	Southwest Atlantic Ocean	Middag et al. (in preparation)	432
GA03	2010	USGT10	North Atlantic	Wu et al. (2014)	91
GA03	2011	USGT11	North Atlantic	Wu et al. (2014)	578
Other expeditions and datasets					
-	1983	VERTEX-IV	North Pacific Ocean	Landing and Bruland (1987)	27
-	2006	EUCFe (*Kilo Moana*)	Pacific Ocean	Slemons et al. (2010)	349
-	2005/2006	CLIVAR P16	Pacific Ocean	Milne and Landing (unpublished data)	174
-	2007	CoFeMUG	South Atlantic	Noble et al. (2012)	429
Total number of dissolved Mn measurements:					5742

Table 4. Observational $[\mathrm{Mn_{diss}}]$ used for comparison with the model simulations. GEOTRACES datasets are indicated by GEOTRACES transect codes. Their accuracies are approved by GEOTRACES on the basis of results of reference samples and cross-over stations. For the other datasets were at the time no reference samples available, or not used for Mn.

ments and are mainly based on different methods by different analysts. Secondly, the West Atlantic Ocean is of importance to the Atlantic meridional overturning circulation, and hence the deep ocean cycling of for example the major nutrients. For these reasons the West Atlantic was chosen as the key site for the $\sim 18\,000$ km long GEOTRACES GA02 transect for the collection of data for dissolved Mn and a suite of other trace elements and isotopes. For these reasons all quantitative arguments in this study concern the West Atlantic GEOTRACES section.

The particulate $[\mathrm{Mn_{ox}}]$ measurements from Landing and Bruland (1987) were used to tune the redox model. The data from the CLIVAR P16 cruise are unpublished; sampling is from the surface up to 1000 m depths; its methods of analysis are described by Milne et al. (2010).

Biogeosciences Discuss., doi:10.5194/bg-2016-282, 2016
Manuscript under review for journal Biogeosciences
Published: 11 July 2016

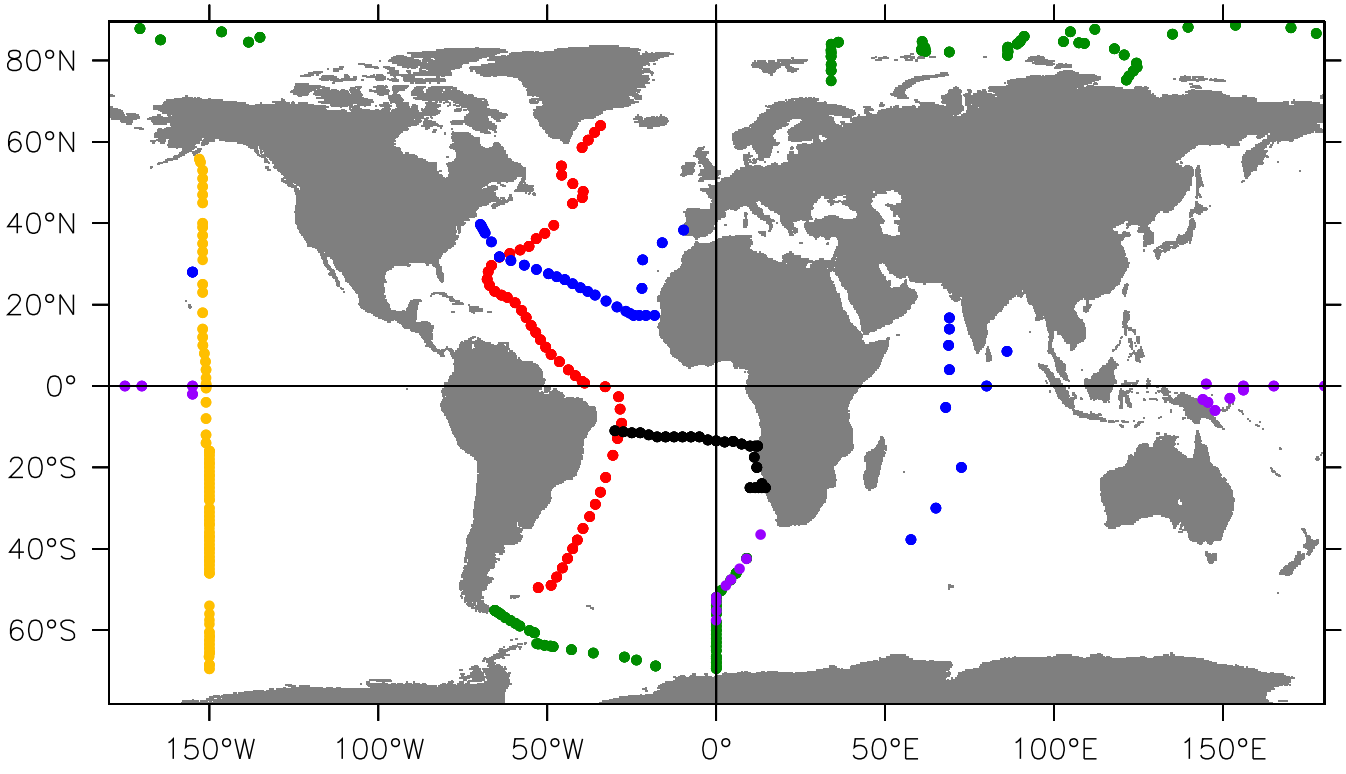

Figure 4. Transect (or expedition) names corresponding to station colours: GIPY11 in the Arctic Ocean; GIPY4 in the Southern Ocean; GIPY5 in the Atlantic sector of the Southern Ocean; GI04 in the Indian Ocean; GA02 in the West Atlantic Ocean; GA03 in the North Atlantic Ocean; VERTEX-4 in the North Pacific Ocean; EUCFe in the equatorial Pacific Ocean; CLIVAR P16 in the Pacific Ocean; CoFeMUG in the South Atlantic Ocean. See Table 4 for an overview with references and the number of observations.

3 Results

3.1 Reference simulation

Figure 5 shows the modelled and measured dissolved Mn concentrations at four depths; observations as coloured dots (same scale). The dissolved Mn concentration is high in the surface of the Atlantic, Indian and Arctic oceans. The order of magnitude is reproduced by the model (Fig. 5a). The model also reproduces the latitudinal gradient of [Mn_{diss}], reflecting dust deposition patterns (Fig. 3a).

Figure 6 shows the dissolved Mn concentrations at full depth in the Zero-Meridian Southern Ocean and the West Atlantic Ocean from the *Reference* simulation; observations as coloured dots. Lower concentrations in the deep ocean are reproduced by the model (Fig. 5b–d and 6). Both the model and observations present a mainly homogeneous distribution of just over 0.1 nM. The generally higher Mn_{diss} concentrations near the surface compared to the deep ocean are caused by a combination of dust deposition and photoreduction. This is mostly captured by the model. Also the penetration of Mn_{diss} from Mn-rich

Biogeosciences Discuss., doi:10.5194/bg-2016-282, 2016
Manuscript under review for journal Biogeosciences
Published: 11 July 2016

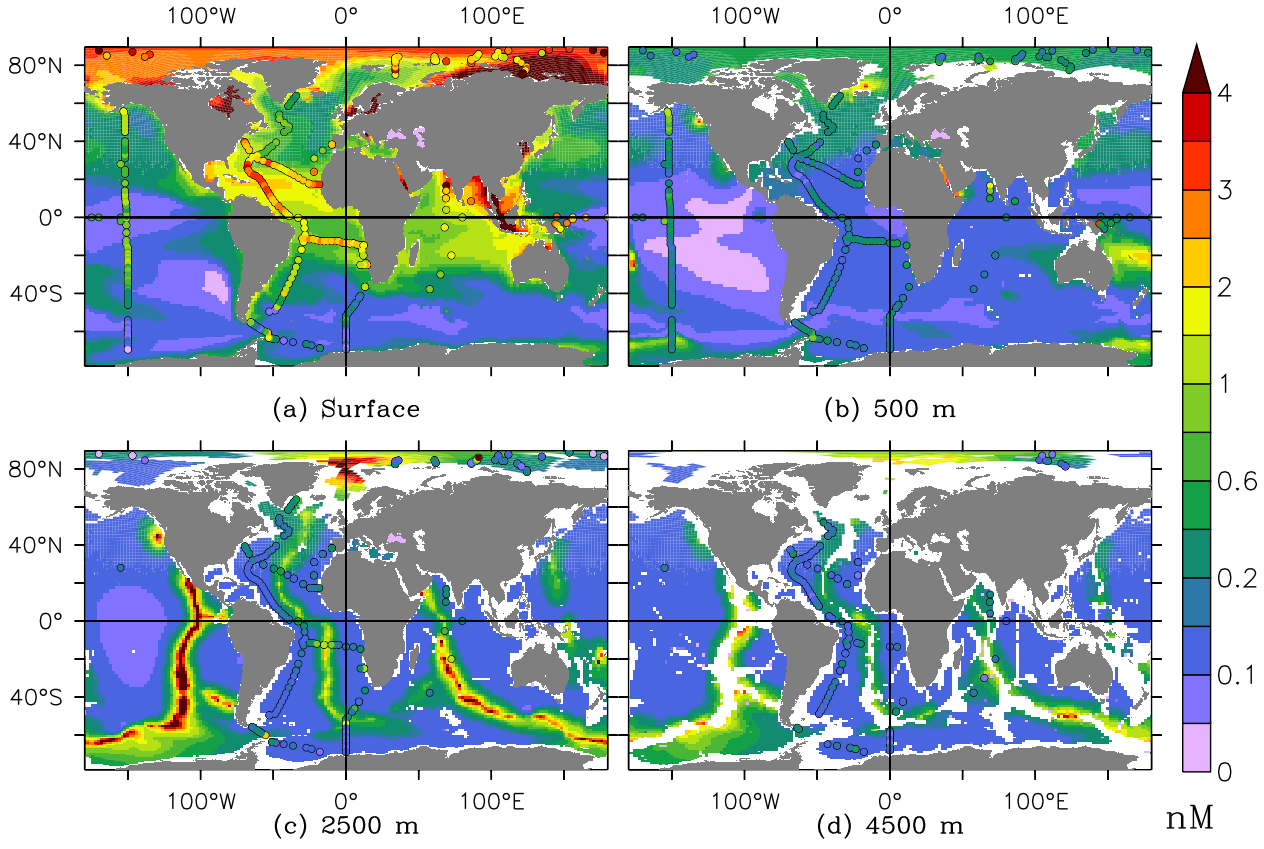

Figure 5. $[Mn_{diss}]$ (nM) at four depth layers in the world ocean for the reference simulation (*Reference*) after 500 yr (annual average). Observations are presented as coloured dots; white is the land mask of the model grid.

surface waters into the deep ocean at around 50° N is reproduced by the model, but this is scavenged quickly before traversing southward in the North Atlantic Deep Water (NADW), which is consistent with early studies (e.g. Bender et al., 1977). Finally, the measurements near hydrothermal vents in the Atlantic and Indian oceans are reproduced by *Reference* (Fig. 5c and 6).

Still, at many places, the Mn_{diss} concentration is underestimated by the model, with the exception of the Southern and Arctic oceans. The underestimation is especially pronounced at the surface of the Atlantic and Pacific oceans (Fig. 5a), as well as at 500 m depth in the Arctic and Pacific oceans and some parts of the Atlantic and Southern oceans (Fig. 5b). Furthermore, the relatively high concentration of Mn_{diss} near the Amazon outflow of the West Atlantic transect is not reproduced.

Figure 7 presents $[Mn_{diss}]$ of the GA03 transect. Observations from Wu et al. (2014) are presented as coloured dots. Again, the general patterns are captured, but the concentration of Mn_{diss} very close to the Mid-Atlantic Ridge is underestimated, while above the ridge (at about 2–3 km depth) it is overestimated. In other words, the modelled hydrothermal Mn_{diss} signal is not as sharp as in the observations. It is probably difficult to improve this feature because of the low vertical resolution of the model

Biogeosciences Discuss., doi:10.5194/bg-2016-282, 2016
Manuscript under review for journal Biogeosciences
Published: 11 July 2016

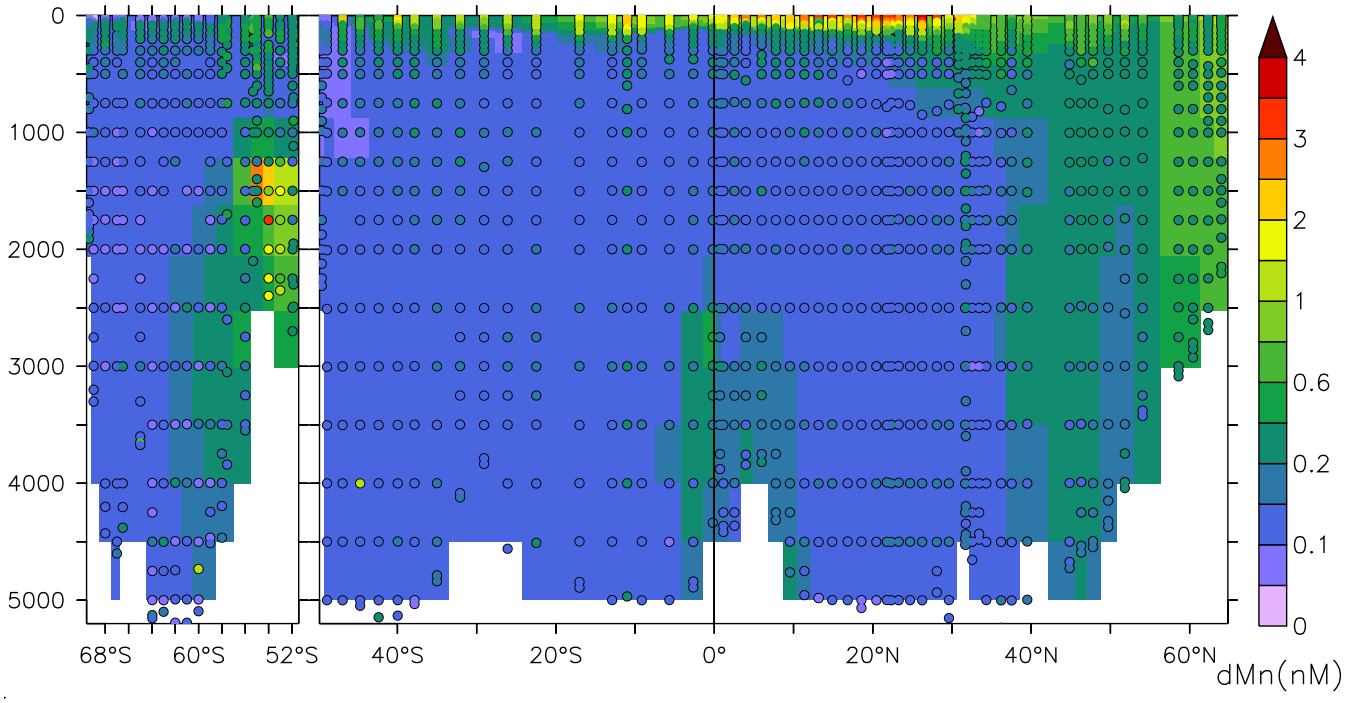

Figure 6. $[Mn_{diss}]$ (nM) at the Zero-Meridian GIPY5_e and the West Atlantic GA02 GEOTRACES transects for *Reference* after 500 yr (annual average). Observations are presented as coloured dots.

Simulation	Correlation	RMS deviation (nM)	Reliability index
Reference	0.72 ($\pm$0.07)	0.40 ($\pm$0.04)	1.82 ($\pm$0.06)
LowHydro	**0.61**	**0.47**	**2.93**
NoThreshold	0.72	0.41	**2.77**

Table 5. Statistical model–data comparison for $[Mn_{diss}]$ at the GEOTRACES West Atlantic GA02 and Zero-Meridian part of the GIPY5 transects. The significance errors in the entries of *Reference* are $\pm 2\sigma$ from Monte Carlo samplings. Bold face values denote significant worsening compared with *Reference*; other values are insignificant.

at that depth. The dissolved Mn concentration is overestimated at the surface as well as near the lateral boundaries (USA, Mauritania, and Portugal).

To more objectively compare the different simulations to each other, we list several goodness-of-fit statistics in Table 5. They compare the model simulations to observational data from the GEOTRACES GA02 and GIPY5 transects. The model–data $[Mn_{diss}]$ correlation coefficient has a value of 0.72 for the *Reference* simulation. The reliability index, the average factor by which model predictions differ from observations, shows that on average the model differs by a factor of 1.82 from observations (Stow et al., 2009, and Appendix B).

Biogeosciences Discuss., doi:10.5194/bg-2016-282, 2016
Manuscript under review for journal Biogeosciences
Published: 11 July 2016

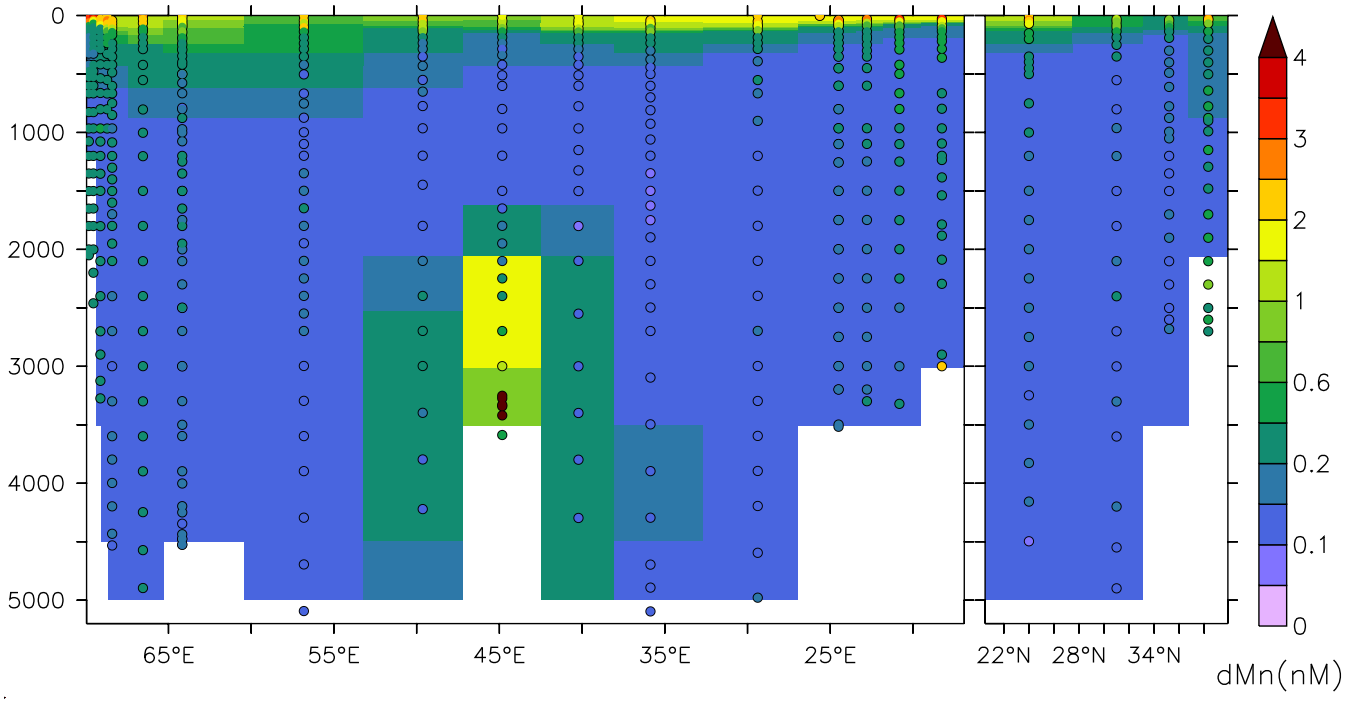

Figure 7. $[Mn_{diss}]$ (nM) at the North Atlantic GA03 GEOTRACES transect for *Reference* after 500 yr (annual average). Observations are presented as coloured dots.

3.2 Reduced hydrothermal flux and export

We have shown that the *Reference* simulation gives a reasonably realistic distribution of the effects of hydrothermal vents and the background concentration in the deep ocean. This is achieved by setting a large Mn_{diss} flux from hydrothermal vents and a big maximum settling velocity at the depth of the vents to remove the hydrothermal Mn away from the source. The simulation presented in this section, *LowHydro*, is meant to test if the high flux is necessary or realistic.

Figure 8 shows the relative change in $[Mn_{diss}]$ at four depths when both the hydrothermal input and the maximum settling velocity are decreased by a factor of 10 (*LowHydro*). In the surface ocean (Fig. 8a) there are both moderate increases and decreases, but there is a very large increase (over 200 %) in the Weddell Sea. In the deep ocean below about 1 km depth such a large increase is not limited to the Weddell Sea but stretches over most of the Atlantic and Indian oceans (Fig. 8c and d). Exceptions are the locations near the oceanic ridges, where there is hydrothermal activity. At those locations $[Mn_{diss}]$ decreased by up to 90 %. Hence, *LowHydro* appears to give a much worse prediction of $[Mn_{diss}]$ than *Reference* does.

The $[Mn_{diss}]$ transects in Fig. 9 also show that *LowHydro* is worse than the *Reference* simulation. For instance, the high $[Mn_{diss}]$ with a clear hydrothermal origin at 54° S has disappeared, while at the same time the deep ocean filled up with Mn_{diss} resulting in a consistent overestimation of about a factor of five in most of the deep West Atlantic Ocean. In the South Pacific Ocean and the Indian Ocean the signature of hydrothermal input of Mn_{diss} is – though smaller and worse than in *Reference* –

Biogeosciences Discuss., doi:10.5194/bg-2016-282, 2016
Manuscript under review for journal Biogeosciences
Published: 11 July 2016

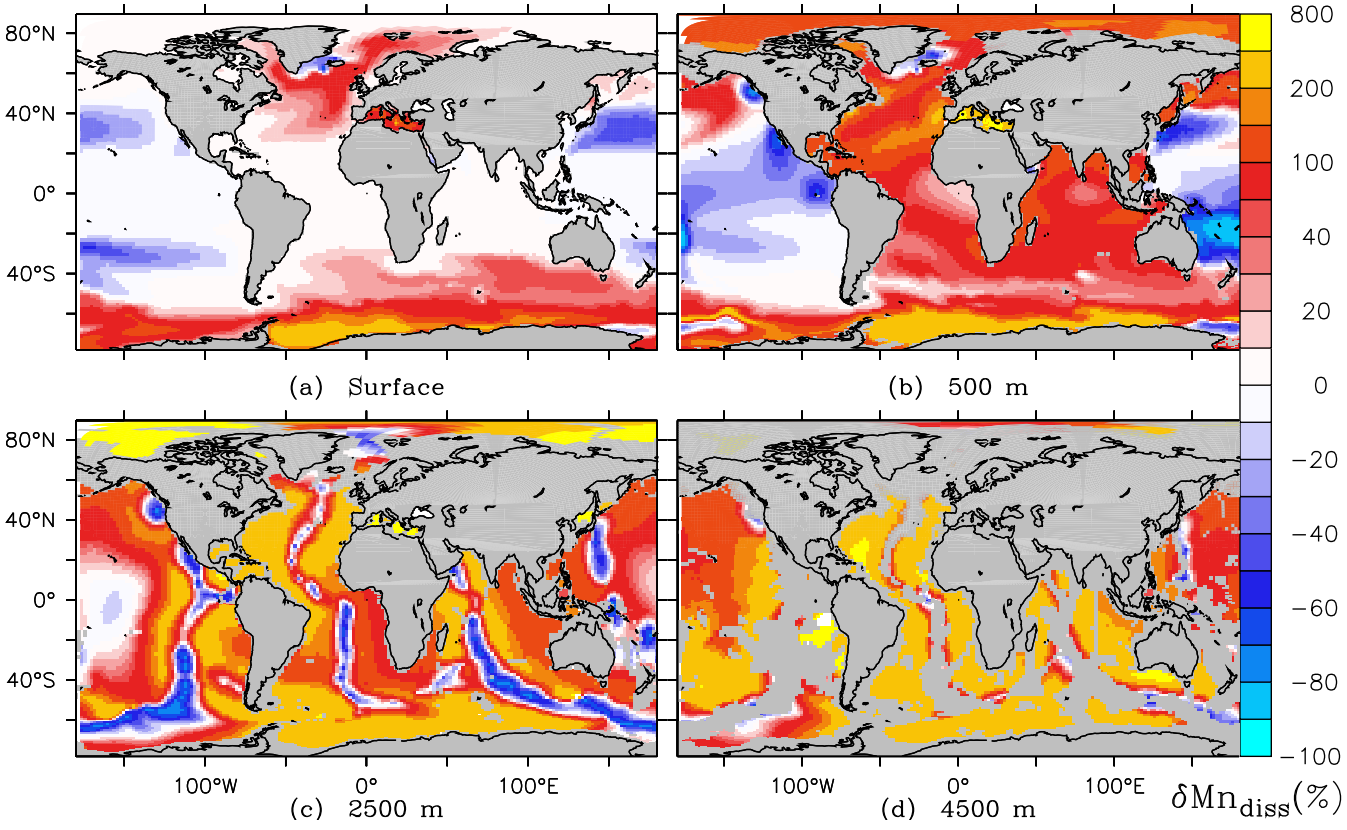

Figure 8. Result from the simulation with hydrothermal vent Mn input decreased and settling velocity decreased (*LowHydro*). Relative difference in $[\mathrm{Mn_{diss}}]$ (%) between *Reference* and *LowHydro*. To represent the changes of much larger than 100 %, the scale is increased from +50 % upwards.

still clearly present, with $[\mathrm{Mn_{diss}}]$ values near the ridges distinctly different from the "background" concentration (results not shown).

Furthermore, the statistics of *LowHydro* compared to *Reference* unambiguously show that $[\mathrm{Mn_{diss}}]$ worsened (Table 5). The *LowHydro* simulation is significantly worse in all three statistics: the gradients from hydrothermal vents have disappeared, and $[\mathrm{Mn_{diss}}]$ is much too high throughout the ocean compared to *Reference*.

3.3 No aggregation threshold

The simulation *NoThreshold* does not impose the $\mathrm{Mn_{ox}}$ condition, meaning that settling occurs unconstrainedly in this simulation (no aggregation threshold). Figure 10 presents $[\mathrm{Mn_{diss}}]$ from *NoThreshold*. In the intermediate and deep ocean south of 40° N, compared to *Reference* (Fig. 6), the concentration of $\mathrm{Mn_{diss}}$ decreases by more than 50 % in much of the ocean.

Neither the correlation coefficient nor the root-mean-square deviation of $[\mathrm{Mn_{diss}}]$ in *NoThreshold* significantly differ from that of *Reference*, because the homogeneous, already low background concentration of $\mathrm{Mn_{diss}}$ is reduced to close to zero,

Biogeosciences Discuss., doi:10.5194/bg-2016-282, 2016
Manuscript under review for journal Biogeosciences
Published: 11 July 2016

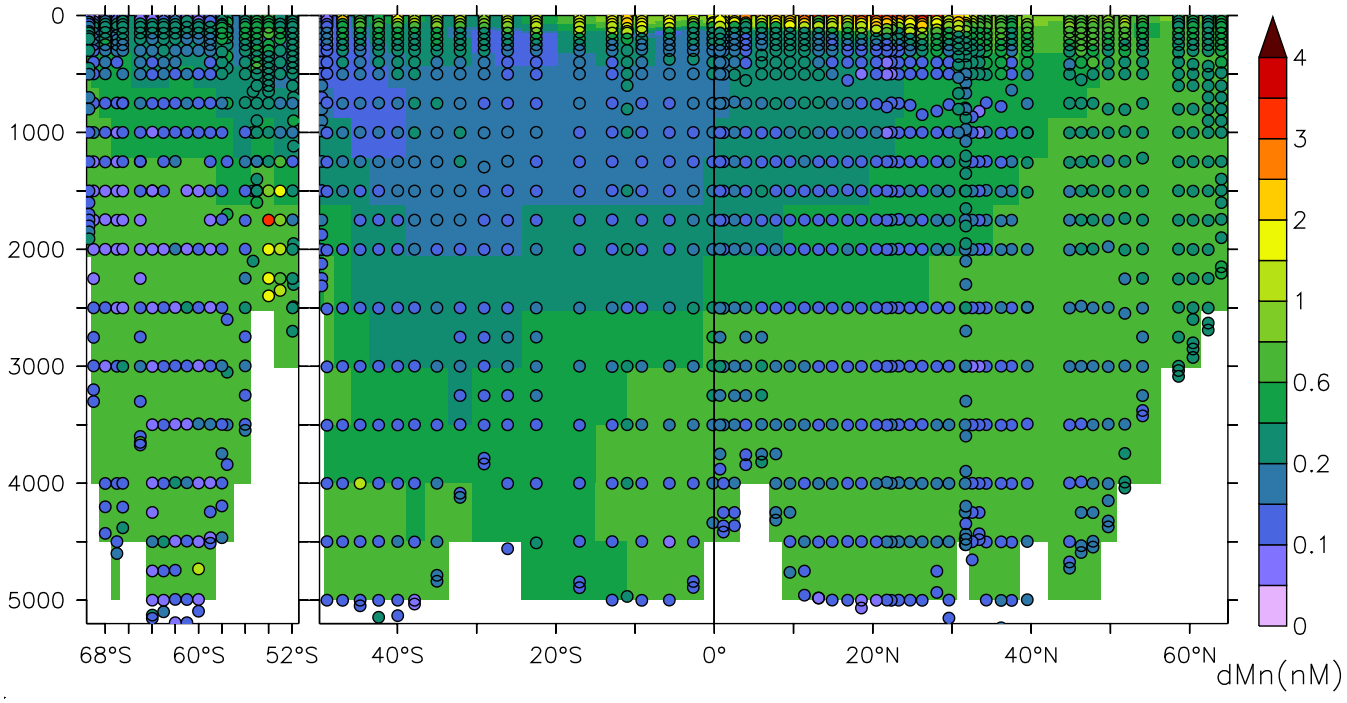

Figure 9. [Mn_{diss}] (nM) from the simulation with hydrothermal vent Mn input decreased and settling velocity decreased (*LowHydro*) at the West Atlantic GA02 and Zero-Meridian Southern Ocean GIPY5_e GEOTRACES transects.

while the hydrothermal signals are still correctly represented in the *NoThreshold* simulation. This means that away from ocean ridges the spatial variation of the modelled [Mn_{diss}] is similar to that of the observations (Stow et al., 2009). However, the reliability index, the average factor by which model predictions differ from observations, has changed from 1.82 to 2.77, which is significant by over thirty standard deviations. Therefore, the *NoThreshold* simulation is much worse than the *Reference* simulation.

4 Discussion

Many of the properties of the Mn_{diss} distribution in the world ocean are reproduced by the *Reference* simulation (Sect. 3.1). Shortcomings of the predicted [Mn_{diss}] are relatively minor. However, some discussion on the assumptions of the underlying processes in the model is required.

4.1 Margin sediments

Here we chose to use a simple sediment flux parameterisation for this study. In our model Mn_{diss} is added to bottom water from anoxic sediments analogously to the iron flux in the model PISCES (Aumont et al., 2015). This first-order approach works well mostly, but shortcomings can be identified.

Biogeosciences Discuss., doi:10.5194/bg-2016-282, 2016
Manuscript under review for journal Biogeosciences
Published: 11 July 2016

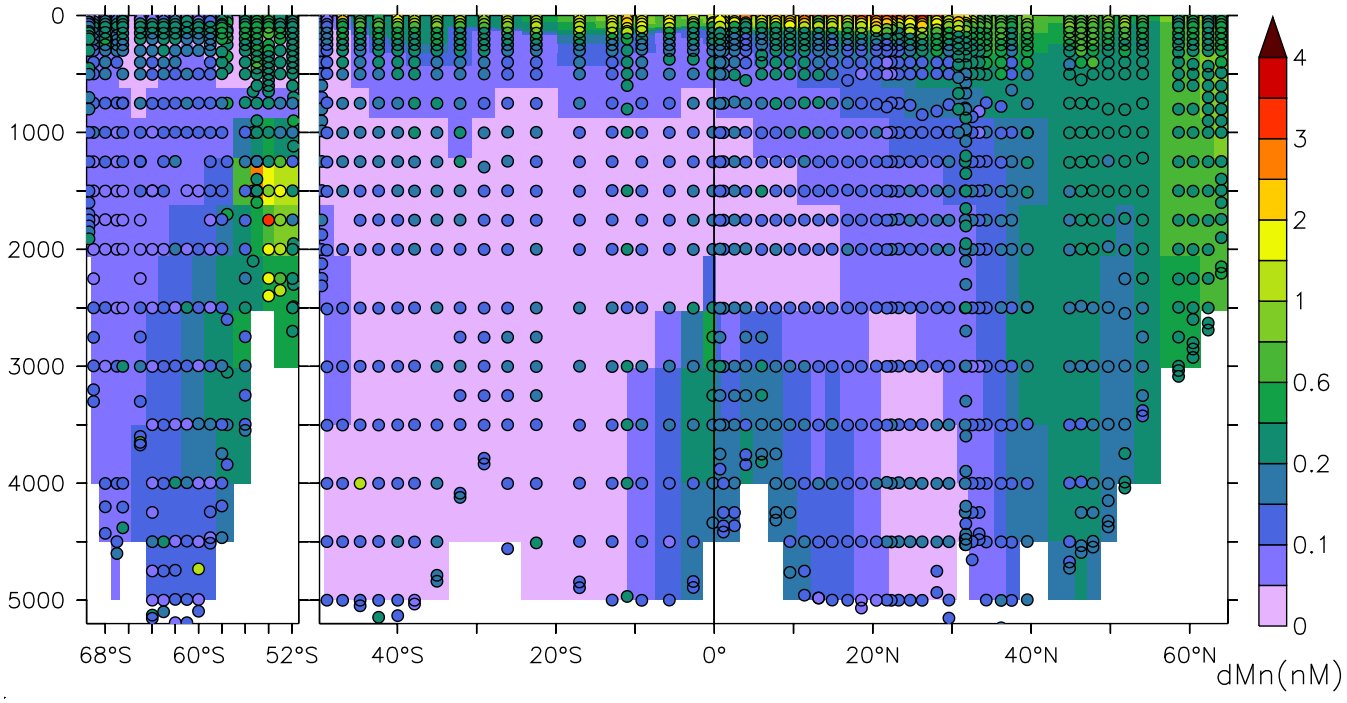

Figure 10. [Mn_{diss}] (nM) at the West Atlantic GA02 and Zero-Meridian Southern Ocean GIPY5_e GEOTRACES transects. Simulation without threshold (*NoThreshold*).

On the one hand, the flux may be overall underestimated, for instance because Mn reduction releases a higher free energy than Fe reduction, so that Mn oxides reduce more easily and hence before Fe reduction takes place (Sarmiento and Gruber, 2006, pp. 232–236). Furthermore, high benthic Mn fluxes have been observed from eastern North Pacific marine sediments (McManus et al., 2012). On the other hand, at some large-shelf regions, like the Arctic Ocean, the Mn flux is overestimated, which is because of the fact that this parameterisation does not handle large shelf regions well.

Slomp et al. (1997) measured pore water concentrations of dissolved Fe and Mn. The Mn/Fe ratios based on their maximum pore water concentrations range from 0.2 to 1.2. Balzer (1982) reports fluxes from sediment to bottom water of dissolved Mn and Fe that yield an average ratio of 0.5. The value that we used, 0.2, is at the lowest end of the reported values. This choice is mainly due to the fact that the crude iron flux parameterisation results in increases that are out of proportion in some regions of the ocean (e.g. the East Arctic Ocean). Besides this, we cannot exclude the possibility of sediment resuspension and subsequent dissolution, akin to aluminium (Van Hulten et al., 2014). Particulate Mn/Fe ratios vary from 0.02 to 0.04 (Bortleson and Lee, 1974; Slomp et al., 1997), about an order of magnitude smaller than our 0.2. These very low particulate Mn/Fe ratios may contribute negatively to the effective dissolved Mn/Fe flux ratio into bottom water. Even if this contribution is very small compared to the total particulate matter pool in the upper sediment, this may still contribute significantly to the dissolved

Biogeosciences Discuss., doi:10.5194/bg-2016-282, 2016
Manuscript under review for journal Biogeosciences
Published: 11 July 2016

pool in the bottom water, because there is much more particulate iron and manganese in the sediment than dissolved (in the porewater).

A higher $\mathrm{Mn_{diss}}$ input would be beneficial for the simulation in the Atlantic and especially the Pacific Ocean where $[\mathrm{Mn_{diss}}]$ is underestimated everywhere but south of 50° S. Underestimation may be due to too strong vertical mixing in the model. However, a high sedimentary input would especially have a big impact on $[\mathrm{Mn_{diss}}]$ in the Arctic Ocean: the area of maximum sediment $\mathrm{Mn_{diss}}$ flux is very large in that region (Fig. 3c). A higher Mn source would result in an overestimation of $[\mathrm{Mn_{diss}}]$ in the Arctic Ocean. This has also been concluded from a sensitivity study by Van Hulten et al. (2013) who used the same parameterisation for aluminium sediment input as for Mn here.

To summarise, we chose to use a simple sediment flux parameterisation for this study. While out of the scope of this study, a better parameterisation, or even an explicit sediment model, could make for a more realistic simulation and should be pursued in future studies.

4.2 Hydrothermal source

In the model, hydrothermal $\mathrm{Mn_{diss}}$ is added to the ocean based on a model proxy of $^3\mathrm{He}$ (Dutay et al., 2004). For *Reference* and *NoThreshold* the $\mathrm{Mn_{diss}}$ addition has been set to 0.10×10^9 mole Mn for each mole of $^3\mathrm{He}$. There is no reference to literature values in Table 2 since they are very uncertain. For instance, Klinkhammer and Bender (1980) note that "Corliss and Dymond (1979) reported that the $\mathrm{Mn}:{}^3\mathrm{He}$ ratios vary by over a factor of 2 in the Galapagos vents, and as we discuss below, similar variations are found at 21° N". Rather a value is chosen to yield an acceptable distribution of $\mathrm{Mn_{diss}}$.

The goal of *LowHydro* is to investigate whether the combination of the high hydrothermal input of $\mathrm{Mn_{diss}}$, and strong aggregation (modelled as a high settling velocity), is needed to get a realistic distribution of $\mathrm{Mn_{diss}}$, namely that of *Reference*. To this end, the choice was made to decrease hydrothermal input and also decrease the settling velocity in *LowHydro*. Decreasing only hydrothermal input would trivially result in a proportionally smaller $[\mathrm{Mn_{diss}}]$ near the vents. The result of decreasing the settling velocity would be relatively trivial as well, namely, much more $\mathrm{Mn_{diss}}$ in the deep ocean. Indeed, in *LowHydro* the spatial distribution of $[\mathrm{Mn_{diss}}]$ becomes more homogeneous. Neither the low background concentration nor the high hydrothermal vent concentrations are reproduced (Fig. 9). Decreasing hydrothermal input and the settling velocity by a smaller factor than 10 results in a $\mathrm{Mn_{diss}}$ distribution that is better than *LowHydro* but not as good as in *Reference* (not presented). In any case, the main result is that the high hydrothermal input used in the *Reference* simulation is needed for a realistic simulation of $[\mathrm{Mn_{diss}}]$.

According to observations a negligible amount of Mn from hydrothermal vents reaches the surface ocean. As Bruland and Lohan (2006) put it: "The hydrothermal input of iron and manganese [...] is essentially all scavenged and removed in the deep sea prior to having a chance to mix back into the surface waters." However, this is what we have thought about iron while there are now doubts about this (Tagliabue et al., 2010). Similarly, hydrothermal Mn may not be completely removed from the ocean before reaching the surface by currents and vertical mixing. There are different potential reasons for this. First, the oxidation of Mn(II) is thermodynamically favoured, but the large activation energy of Mn(II) oxidation renders Mn(II) stable in aquatic environments (Nealson, 2006). In our model we made a choice in assuming that the activation energy is not an issue, and the background "dissolved" Mn particles are not $\mathrm{Mn^{2+}}$ ions but rather suspended colloids or complexes. Candidates include

Biogeosciences Discuss., doi:10.5194/bg-2016-282, 2016
Manuscript under review for journal Biogeosciences
Published: 11 July 2016

colloidal $\mathrm{Mn_{ox}}$ and Mn bound to ligands, respectively the second and third potential reasons for the observed background "$\mathrm{Mn_{diss}}$" concentration. The low $\mathrm{Mn_{diss}}$ concentrations away from hydrothermal vents are established in our model by removing the high hydrothermal Mn input down to a certain concentration.

Interestingly, in this way, in *Reference*, hydrothermal flux accounts for 64 % of the total Mn input. Dust deposition is two times as small as hydrothermal input, and still $[\mathrm{Mn_{diss}}]$ in the upper 1000 m of the ocean is dominated by Mn dissolution from deposited dust and $\mathrm{Mn_{diss}}$ release from marginal sediments. The reason for this is that in the model the settling velocity of $\mathrm{Mn_{ox}}$ is much higher near hydrothermal vents (up to $10\ \mathrm{m\,d^{-1}}$) than in the surface ocean ($1\ \mathrm{m\,d^{-1}}$). The modelling study by Lavelle et al. (1992) suggests a settling velocity much higher than our w_{ox}. They used a model with an additional tracer of large particles (aggregate products) that had settling speeds of up to $175\ \mathrm{m\,d^{-1}}$ (near hydrothermal vents, as they model those regions). This shows that there is justification in using an increasing settling velocity, but also that at least two particle tracers may be needed in the model. It is worth investigating in future studies if this would make for a more realistic and useful model.

4.3 Biological cycle

Our model does not include biological processes involving manganese, because at the moment there is not enough data available that would constrain these processes. Specifically, while Mn correlates well with the nutrients $\mathrm{PO_4}$ and $\mathrm{NO_3}$ (Middag et al., 2011a), there is no clear evidence for typical uptake-remineralisation processes. On the one hand, of course, Mn plays in important role in biology. It even limits primary production in parts of the Southern Ocean (Coale, 1991; Middag et al., 2011a, 2013; Browning et al., 2014), although the micro-nutrient iron often appears more significant (Buma et al., 1991). This is even suggested by our model–data comparison: at the Zero-Meridian GIPY5_e transect south of 62° N, $\mathrm{Mn_{diss}}$ is depleted at the surface, but between $\sim 50\ \mathrm{m}$ to $250\ \mathrm{m}$ there is a maximum of $[\mathrm{Mn_{diss}}]$ that may very well be due to remineralised plankton (Fig. 6, left transect). The maximum is only visible in the observations (Middag et al., 2011a), which suggests that a remineralisation process of Mn is missing in the model. On the other hand, this does not mean that primary production always has an important impact on the dissolved manganese concentration (not identified in the West Atlantic transect, Fig. 6, right transect). If future studies will show that the impact is higher than here assumed, and it is due to biological incorporation, this process should be included in future versions of the model. Possibly, limitation of $\mathrm{Mn_{diss}}$ for the growth of phytoplankton, and co-limitation with iron in the Southern Ocean, plays an important role for the carbon cycle (Peers and Price, 2004; Middag et al., 2013). Hence, such a limitation function could be added to carbon cycle models as well.

4.4 Redox rates

In our model, oxidation takes place everywhere with the same $k_{\mathrm{ox}} = 0.341 \times 10^{-3}\ \mathrm{h^{-1}}$. Based on the underestimation of the concentrations in the surface of the Atlantic and Pacific oceans, one may think that $[\mathrm{Mn_{ox}}]$ is too high compared to $[\mathrm{Mn_{diss}}]$. In other words, assuming approximate equilibrium, the ratio $k_{\mathrm{ox}}/k_{\mathrm{red}}$ could be too high. However, the k values in our model are optimised to get values consistent with the ratio of concentration measurements of $\mathrm{Mn_{ox}}$ and $\mathrm{Mn_{diss}}$. Figure 11 shows the $\mathrm{Mn_{ox}}$/$\mathrm{Mn_{diss}}$ concentration ratio of the *Reference* simulation. The left panel shows that this ratio is less than 0.001 in the upper

Biogeosciences Discuss., doi:10.5194/bg-2016-282, 2016
Manuscript under review for journal Biogeosciences
Published: 11 July 2016

100 m, and the deep ocean (right panel) shows a value of about 0.2; both values are consistent with the VERTEX-IV cruise date from Bruland et al. (1994) (red squares).

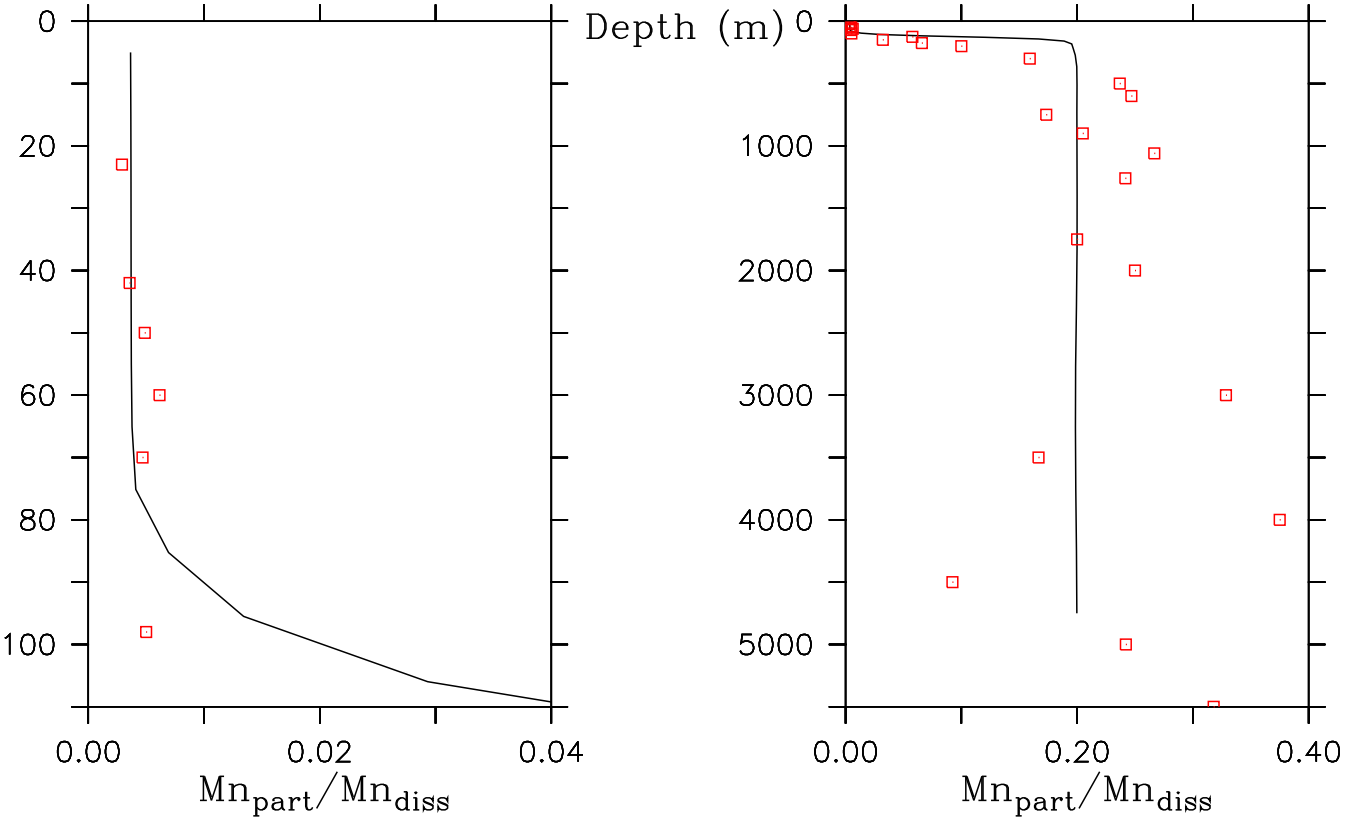

Figure 11. $[Mn_{part}]/[Mn_{diss}]$ in the Pacific Ocean from the VERTEX-IV station in the upper 110 m (left) and at full depth (right). Red squares are observations; the black line is the *Reference* simulation.

Generally, the modelled $[Mn_{part}]/[Mn_{diss}]$ lies at the lower end of the observed ratio, while only between 100 and 400 m there may be an overestimation of particles compared to dissolved Mn. In any case, adjusting the first-order rate constants with any reasonable amount does not result in a sufficiently high $[Mn_{diss}]$ (results not presented).

One may introduce a threshold on the oxidation process instead of the settling of the particles. In that case, oxidation only takes place when higher than 0.1 nM (k_{ox} is multiplied by $H(\mathcal{X}-0.1\ \mathrm{nM})$). While this yields a reasonable distribution of Mn_{diss} (not significantly worse than *Reference*), the Mn_{ox}/Mn_{diss} concentration ratio below 250 m is then strongly underestimated compared to the VERTEX data (Fig. 12, not discussed elsewhere in the paper). This pleads for using an aggregation rather than an oxidation threshold.

Biogeosciences Discuss., doi:10.5194/bg-2016-282, 2016
Manuscript under review for journal Biogeosciences
Published: 11 July 2016

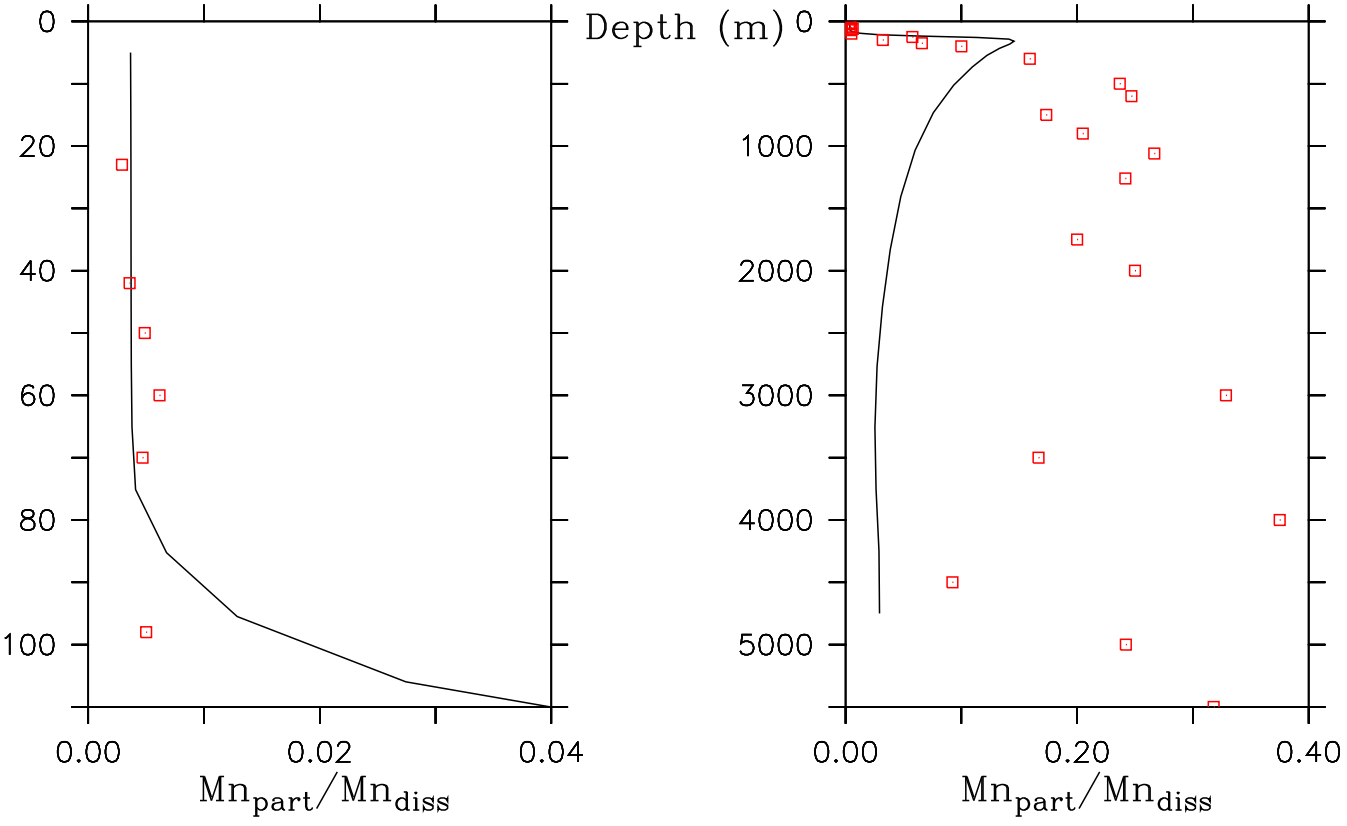

Figure 12. $[Mn_{part}]/[Mn_{diss}]$ in the Pacific Ocean from the VERTEX-IV station in the upper 110 m (left) and at full depth (right). Red squares are observations; the black line is the *Reference* simulation.

4.5 Export dynamics

In the *NoThreshold* simulation $[Mn_{diss}]$ is underestimated in much of the ocean. When removing the threshold, the RMSD significantly worsens: it appears that the threshold is needed to reasonably simulate $[Mn_{diss}]$. But there are several alternatives to the aggregation threshold that may keep $[Mn_{diss}]$ in check.

Firstly, instead of an aggregation threshold, a criterion on oxidation may be imposed, because, hypothetically, there may be a lower limit below which oxidising microbes would not proliferate and the pseudo-first-order rate constant would then be lower. A simulation with an oxidation threshold based on this idea gives similar results as the aggregation threshold, but as we saw in the previous section, it would influence significantly the Mn_{ox}/Mn_{diss} ratio in the deep ocean, making for a less realistic simulation. Therefore, this alternative should probably not pursued.

Secondly, the process of oxidation is strongly mediated by adsorption onto particles, after which it forms larger aggregates that settle faster. This is now parameterised by increasing the settling velocity of particles with depth. However, a more explicit model for adsorption/desorption may be useful. Possibly much of the Mn_{ox} does not settle; then another tracer of adsorbed

Biogeosciences Discuss., doi:10.5194/bg-2016-282, 2016
Manuscript under review for journal Biogeosciences
Published: 11 July 2016

Mn is needed that would export oxidised Mn (in adsorbed or aggregated form). The adsorption should not take place onto a homogeneous pool of particles as is effectively done in our model, but rather onto e.g. calcium carbonate ($CaCO_3$) (Martin and Knauer, 1983; Fraústo da Silva and Williams, 2001) or lithogenic particles (Roy-Barman, 2009). Sediment samples show a strong correlation between manganese and lithogenic particles, while Mn does not show any correlation with biogenic silica, POC or $CaCO_3$ according to recent observations and modelling (Roy-Barman, 2009). On the one hand, this suggests that only lithogenic particles are a scavenger of Mn. On the other hand, we do not know whether the correlation comes from Mn adsorption onto lithogenic particles, or if it is lithogenic on itself.

Thirdly, oxidation is mediated by microbes (mainly bacteria) (Sunda and Huntsman, 1994; Von Langen et al., 1997; Tebo et al., 2005; Fraústo da Silva and Williams, 2001). Possibly they prolong the time of Mn_{ox} particles spent in the euphotic zone, but this has not been tested. In the model we assume that these are included in the redox rate constant. As of yet, there are no oxidising microbes in our model. If we want the redox rate constants to depend on inhomogeneously distributed quantities like the bacterial distribution or the oxygen concentration, the equations may need to be modified, and our model may need to be extended. If this is done, more Mn may stay suspended ('dissolved Mn') as a consequence.

Fourthly, there have been suggestions that Mn ligands keep Mn in solution (Sander and Koschinsky, 2011; Madison et al., 2013). That would result in less conversion to manganese oxide aggregates, and hence may solve the removal problem, but this may yield wrong Mn_{ox}/Mn_{diss} concentration ratios like in the previous section. Similarly, colloids, which have a size that falls within the operationally defined dissolved Mn, keep Mn floating as long as they do not aggregate.

5 Conclusions

This is the first study in which the 3-D distribution of Mn_{diss} has been modelled. The distribution of Mn_{diss} is captured reasonably well by our model when compared to the recent observations from the GEOTRACES programme. A combination of photoreduction and Mn sources to the upper ocean mostly yields the high surface concentrations of manganese. However, they are somewhat underestimated by the model, which may be due to too low surface Mn input or a too strong sink (among which settling), both of which are uncertain and could therefore be adjusted for a more realistic simulation. The most important sources for the upper ocean are dust, then sediments, and, more locally, rivers, whereas hydrothermal vents are the most important in the deep ocean. The observed sharp hydrothermal signals are produced by assuming both a high source and a strong removal of Mn near hydrothermal vents. Our model further shows that the Mn at the surface in the Atlantic Ocean moves downwards into the North Atlantic Deep Water, but because of strong removal the Mn signal does not propagate southwards.

There is a mainly homogeneous background concentration of dissolved Mn of about 0.10 nM to 0.15 nM throughout most of the deep ocean. Our model reproduces this by means of a threshold on solid manganese oxides of 25 pM, suggesting that a minimal concentration of particulate Mn is needed before aggregation and removal become efficient. An aggregation threshold, as applied in our model, appears reasonable, and does not affect the modelled Mn_{ox}/Mn_{diss} concentration ratio. An oxidation threshold is more troublesome as it affects this ratio in a negative way. Since the settling condition as a sole threshold already appears to solve most of the removal issue, it is reasonable to further develop the model with the aggregation threshold

Biogeosciences Discuss., doi:10.5194/bg-2016-282, 2016
Manuscript under review for journal Biogeosciences
Published: 11 July 2016

and without the oxidation threshold. Still, the simplified redox and subsequent settling of $\mathrm{Mn_{ox}}$ could be incomplete, or too imprecise, as future studies might show.

Specific scavengers, among which, lithogenic particles and $\mathrm{CaCO_3}$ may play an important role in the removal of $\mathrm{Mn_{diss}}$. Since accounting for these sinks could alter the structure of $[\mathrm{Mn_{diss}}]$ throughout the ocean a lot, this would imply it be necessary to make other fundamental changes in the model as well. At any rate, including these scavenging processes should be considered for future simulations.

Our model does not include biology, because at the moment there is no clear evidence for typical uptake-remineralisation processes as for iron. If future studies show that such a process has a significant impact on the $\mathrm{Mn(II)}$ concentration, biological incorporation should be included in future versions of the model. Besides processes in the photic zone, it may also be needed to model microbial activity throughout the ocean, as that is not homogeneously distributed. This means that our chemical first-order reaction may be insufficient for many modelling purposes.

Hydrothermal fluxes of Mn were set to such a high rate that we must assume $96\,\%$ is scavenged near the outflow of the vents. This choice was made to account for the local high $\mathrm{Mn_{diss}}$ near the oceanic ridges. This is combined with a high w_{ox} in the deep ocean to prevent too much hydrothermal $\mathrm{Mn_{diss}}$ spreading far away from the oceanic ridges. As an alternative, settling may not need to be set as high as $10\ \mathrm{m\,d^{-1}}$ in the deep ocean, but then it is unclear how to simulate the local nature of $[\mathrm{Mn_{diss}}]$ anomalies near the ocean ridges. One possibility is to include extra species of Mn, that may include a very fast sinking particle and a very reactive Mn species.

Process studies of Mn are necessary to determine the rate constants, and possibly thresholds, for redox, scavenging and aggregation. More measurements of particulate $\mathrm{Mn_{ox}}$ concentrations would be useful as well. When measuring $\mathrm{Mn_{ox}}$ it needs to be clear what is measured exactly. It would for instance be useful if (1) a range of particle sizes was measured, and (2) a structural analysis of the particles was performed, such that one can unambiguously say onto which particle Mn is adsorbed or into which particle it is incorporated.

Appendix A: Shipboard methods

A1 Sample collection

For the determination of tracer concentrations, notably dissolved aluminium and dissolved manganese, samples were collected along the GEOTRACES Atlantic Meridional GA02 transect of the Netherlands (Fig. 4). Sampling was done with an all-titanium ultraclean CTD sampling system for trace metals (De Baar et al., 2008) with novel PVDF samplers (Rijkenberg et al., 2015; Middag et al., 2015). Immediately upon recovery, the complete titanium frame with its 24 PVDF samplers was placed inside a clean room environment sampling from where the sub-samples for trace metal analysis were collected. The water was filtered from the PVDF samplers over a $0.2\ \mu\mathrm{m}$ filter cartridge (Sartobran-300, Sartorius) under pressure (1.5 atm) of (inline prefiltered) nitrogen gas. Sub-samples for dissolved metals were taken in cleaned (Middag et al., 2009, for cleaning procedure) LDPE sample bottles. All sample bottles were rinsed five times with the sample seawater. Seawater samples were acidified with HCl to a concentration of 0.024 M HCl which results in a pH of 1.7 to 1.8 with Baseline® Hydrochloric Acid (Seastar Chemicals Inc.).

Biogeosciences Discuss., doi:10.5194/bg-2016-282, 2016
Manuscript under review for journal Biogeosciences
Published: 11 July 2016

A2 Analysis of dissolved Mn

Analyses of dissolved manganese were performed on shipboard with the method developed by Doi et al. (2004) with some slight modifications in the preparation and brands of the chemicals used. Furthermore, samples were buffered in-line with an ammonium borate sample buffer (see text below). Samples were acidified with the equivalent of 2 ml 12 M ultraclean HCl (Baseline® Hydrochloric Acid, Seastar Chemicals Inc.) per litre of sample to 0.024 M HCl which results in a pH of ∼1.8 at least 6 h before analysis. In the flow injection system, the samples were buffered in-line to a pH of 8.5 ± 0.2 with ammonium borate sample buffer. This buffer was produced by dissolving 30.9 g of boric acid (Suprapure, Merck) in 1 L MQ water (Millipore Milli-Q) deionised water $R > 18.2\ \mathrm{M\Omega cm^{-1}}$ and adjusting the pH to 9.4 with ammonium hydroxide (Suprapure, Merck).

The buffered sample was pre-concentrated during 150 s on a Toyopearl AF-Chelate 650M (TosoHaas, Germany) column. Hereafter the column was rinsed for 60 s with MQ water to remove interfering salts. The Mn was subsequently eluted from the column for 200 seconds with a solution of 0.1 M three times quartz distilled formic acid (reagent grade, Merck) containing 0.1 M hydrogen peroxide (Suprapure, Merck) and 12 mM ammonium hydroxide (Suprapure, Merck). The pH of this carrier solution was adjusted to 2.9 ± 0.05. The eluate with the dissolved Mn passed a second column of immobilised 8-hydroxyquinoline (Landing et al., 1986) to remove interfering iron ions in the carrier solution (Doi et al., 2004). Hereafter the carrier mixed with 0.7 M ammonium hydroxide (Suprapure Merck) and a luminol solution. The latter luminol solution was made by diluting 600 µl luminol stock solution and 10 µl TETA (triethylenetetramine, Merck) in $1\ \mathrm{dm^3}$ MQ. The luminol stock solution was made by diluting 270 mg luminol (3-aminophtalhydrazide, Aldrich) and 500 mg potassium carbonate in 15 ml MQ. The resulting mixture of carrier solution, ammonium hydroxide and luminol solution had a pH of 10.2 ± 0.05 and entered a 3 m length mixing coil placed in a water bath of 25 °C. Hereafter the chemiluminescence was detected with a Hamamatsu HC135 Photon counter. Concentrations of dissolved Mn were calculated in nanomole per litre (nM) from the photon emission peak height of triplicate measurements.

The system was calibrated using standard additions from a 5000 nM Mn stock solution (Fluka) to filtered acidified seawater of low Mn concentration that was collected in the sampling region. A five-point calibration line (0, 0.1, 0.2, 0.6 and 1.2 nM standard additions) and blank determination were made every day. The three lowest points (0, 0.1 and 0.2 nM) of the calibration line were measured in triplicate and the two highest points (0.6 and 1.2 nM) in duplicate in order to add more weight to the lower part of the calibration line. The blank was determined by measuring acidified MQ which was below the detection limit and subsequently no blank was substracted. The limit of detection defined as three times the standard deviation of the lowest value observed was < 0.01 nM. The flow injection system was rinsed every day with a 0.5 M HCl solution.

An internal reference sample was measured in triplicate every day. This was a sub-sample of a $25\ \mathrm{dm^3}$ volume of filtered seawater that was taken at the beginning of Leg 1 (also used during Leg 2, i.e. Iceland to the equator) and Leg 3 (Punta Arenas, Chile, to the equator). The relative standard deviation (i.e. the precision) of this replicate analysis seawater sample that was analysed 40 times on different days in triplicate was 2.57 % (Leg 1 and 2) and 1.21 % for 17 analyses during Leg 3. The relative standard deviation on single days was on average 1.37 % and the absolute values were 0.45 and 0.61 nM for the first two legs and Leg 3, respectively.

As external comparison the international reference samples collected on the GEOTRACES Intercalibration Cruise (www.geotraces.org) as well as from the SAFe cruise (Johnson et al., 2007) were analysed for Mn. At the cross-over station we obtained the results listed in Table A1. The dissolved Mn data at the Bermuda Atlantic Time-series Study (BATS) from the GEOTRACES cruises by Royal Netherlands Institute for Sea Research (NIOZ) were checked for accuracy by comparison with the consensus values calculated from an independent referee. This lab had received reference values from the cross-sections of different cruises, including the values that were determined by NIOZ. These

Biogeosciences Discuss., doi:10.5194/bg-2016-282, 2016
Manuscript under review for journal Biogeosciences
Published: 11 July 2016

Mn_{diss} (nmol kg^{-1})	Consensus	Middag et al.	Wu et al. (2014)
SAFe S	0.79 ± 0.06	0.82 ± 0.02	0.79 ± 0.01 $(n = 24)$
SAFe D2	0.35 ± 0.05	0.33 ± 0.01 $(n = 24)$	0.35 ± 0.05 $(n = 28)$
GEOTRACES S	1.46 ± 0.14	1.47 ± 0.03 $(n = 10)$	–
GEOTRACES D	0.21 ± 0.03	0.18 ± 0.01 $(n = 5)$	–

Table A1. The results of external reference samples as reported by NIOZ and by Wu et al. (2014) in context of their datasets reported for the BATS station.

reference values were averaged, resulting in a consensus value, which is here considered as the true value. These values are listed in Table A1, together with the values determined by NIOZ. The distributions of the measurements from NIOZ lie within the precision of the consensus values (the consensus values here are determined from multiple values while a "true value" would be only one value).

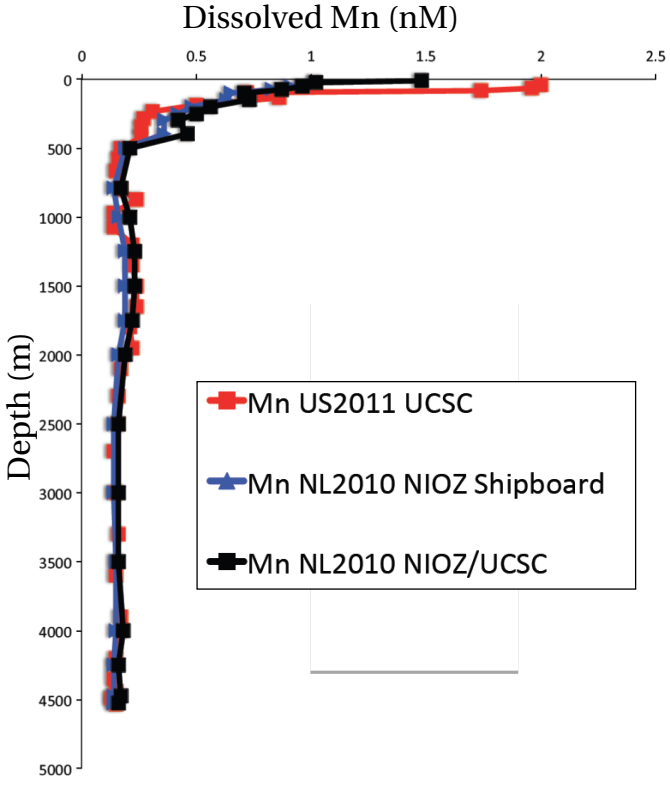

Figure A1. [Mn_{diss}] at the NL 2010 and the US 2011 occupation (Bermuda) station: good agreement between two different methods of two labs with independent primary lab standards prepared by Rob Middag at NIOZ and Geoffrey Smith at UCSC. Samples were analysed by Rob Middag both at sea (FIA NIOZ) and in the lab (ICPMS UCSC).

Biogeosciences Discuss., doi:10.5194/bg-2016-282, 2016
Manuscript under review for journal Biogeosciences
Published: 11 July 2016

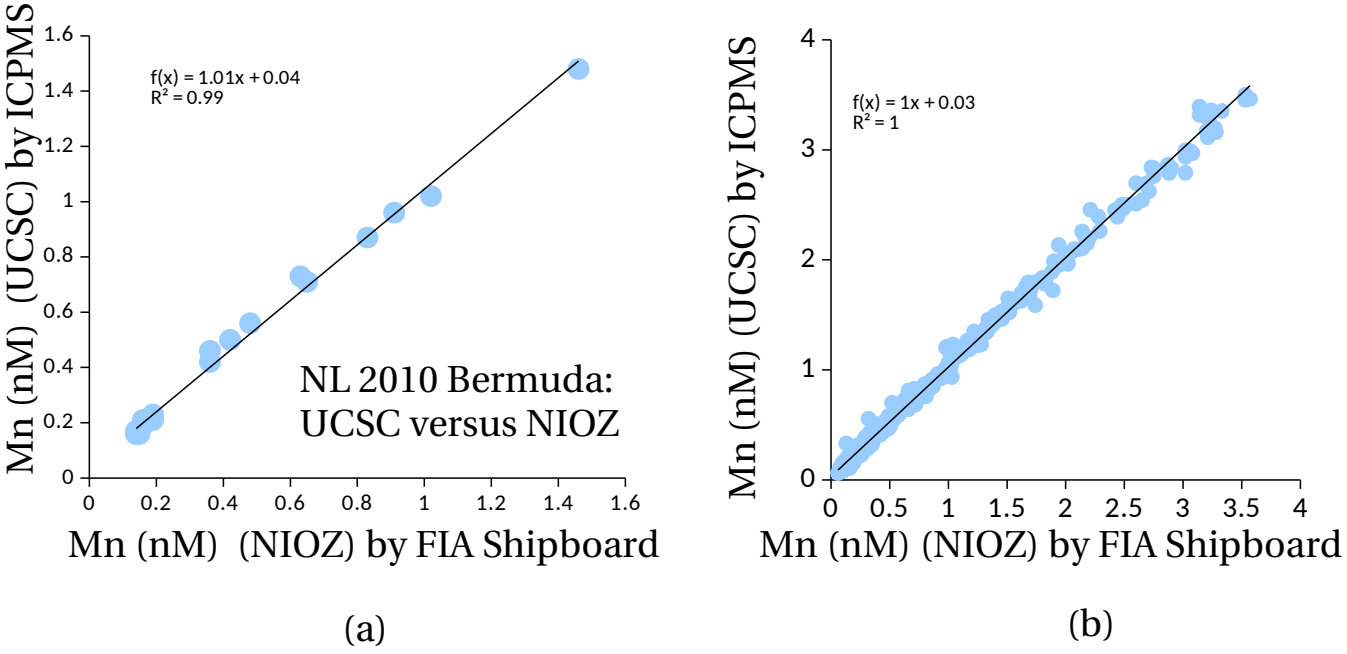

Figure A2. The correlation between the two methods of analysis for the determination of $[\mathrm{Mn_{diss}}]$, shipboard and laboratory mass spectrometry: (a) at Bermuda; (b) all 55 West Atlantic stations

Besides the good agreement with the consensus values, the measurements also agreed well with those of an independent lab. The profiles of both laboratories at BATS are presented in Fig. A1. The difference between the two profiles is significant mostly in the mixed layer. Furthermore, these Mn profiles are also consistent with the profiles determined by Landing et al. (1995).

Figure A2 shows the correlation between the two methods of analysis for the determination of $[\mathrm{Mn_{diss}}]$, shipboard and laboratory measurements, by NIOZ. There is a very good agreement between the shipboard and mass spectrometer analyses, which strongly suggests a high observational accuracy. In this study we used the observational data obtained from the shipboard FIA for the comparison with the model simulations.

These data, and those of Wu et al. (2014), can be found online in the GEOTRACES Intermediate Data Product (IDP) (Mawji et al., 2015).

Appendix B: Data–model comparison

To compare quantitatively the model results of this study with the observations, the focus is on the West Atlantic and Zero-Meridian Southern oceans (GA02 and GPIY4). The data points of the GEOTRACES transects in those regions are used. First the model output is horizontally interpolated onto the station coordinates, keeping the vertical model grid (10 m at the surface up to 500 m thickness near the bottom). Then the model output that lies closest to each of the observations are associated with each other. To be precise, for each observation, we take the shallowest gridbox whoes upper bound lies deeper than the observation, after which residuals can be defined as $P_i - O_i$, where O_i is the observed and P_i the modelled $[\mathrm{Mn_{diss}}]$, for each $i \in \{1, ..., N\}$, with N the number of data points. The interpolation introduces a

Biogeosciences Discuss., doi:10.5194/bg-2016-282, 2016
Manuscript under review for journal Biogeosciences
Published: 11 July 2016

representative error that is taken to be part of the residual (Van Hulten, 2014). Then several statistics are determined, namely the Root Mean Square Deviation (RMSD), the Reliability Index (RI) and the correlation coefficient r.

In addition to classical statistical indices (r, RMSD), another additional performance indicator has been used as suggested in previous skill assessment studies (Stow et al., 2009; Vichi and Masina, 2009): The reliability index (Leggett and Williams, 1981). The reliability index "quantifies the average factor by which model predictions differ from observations". (Stow et al., 2009). It is in essence the root-mean-square deviation, but it uses the logarithm of the residual. This is useful when both large and small values need to be considered (as for this case). The RI is given by

$$RI = \exp\sqrt{\frac{1}{N}\sum_{i=1}^{N}\left(\log\frac{O_i}{P_i}\right)^2}. \tag{B1}$$

where O_i is the measured concentration with index i, P_i is the model prediction associated to the respective observation i, and N is the number of observations.

Furthermore, for each sensitivity simulation the significance of the change in each goodness-of-fit statistic compared with the corresponding reference simulation is calculated. This is determined by means of a Monte Carlo simulation on the reference simulation for which a subsample of 400 has been randomly selected from the original set of 1800 or 1650 data–model points. They are the pairs of observations and model output, both on the model grid. This is done 50 000 times, and from this the 2σ confidence interval is calculated (the mean $\pm$ two times the standard deviation). Suppose that we wish to simulate q, and assume q is in steady state. Given a simulation X, for each model simulation Y resulting in $q_Y(\mathbf{x})$, the average RMSD of the Monte Carlo simulation of $q_Y(\mathbf{x})$ must be outside the 2σ confidence range of the RMSD distribution of $q_X(\mathbf{x})$ to say that Y is a significant improvement or worsening compared to X.

For the visual comparison between model and observations, horizontal and vertical cross-sections of the model data are plotted. Using the same colour scale, observations are plotted as coloured dots to directly compare the model with the observations. Horizontal $[\mathrm{Mn_{diss}}]$ sections are presented for four different depths, where "surface" signifies the average over the upper $45\ \mathrm{m}$, "$500\ \mathrm{m}$" is 400–600 m averaged, '$2500\ \mathrm{m}$' is 2100–2900 m averaged and '$4500\ \mathrm{m}$' is 4000–5000 m averaged. The colour scale is not linear to better show the main features at both low and high concentrations of $\mathrm{Mn_{diss}}$. The vertical $[\mathrm{Mn_{diss}}]$ sections are calculated from the 3-D model data by converting the ORCA2 gridded model data to a rectilinear mapping and interpolating the rectilinear data onto the cruise track coordinates.

Acknowledgements. We would like to thank several people in particular who helped in different ways in this study. Angela Milne and William Landing kindly provided their manganese data from the Pacific Ocean. We want to thank Caroline Slomp, Catherine Jeandel and Micha Rijkenberg for the useful discussion. This research was funded by the NWO (grant 839.08.410; GEOTRACES, Global Change and Microbial Oceanography in the West Atlantic Ocean and grant 820.01.014 GEOTRACES Netherlands-USA Joint Effort on Trace Metals in the Atlantic Ocean). This study was partly supported by a Swedish Research Council grant (349-2012-6287) in the framework of the French-Swedish cooperation in the common research training programme in the climate, environment and energy agreement between VR and LSCE, for the project "Particle transport derived from isotope tracers and its impact on ocean biogeochemistry: a GEOTRACES project in the Arctic Ocean". The sampling and analysis of the data of Milne and Landing (unpublished data) was supported by NSF grants OCE-0223378, OCE-0550317 and OCE-0649639.

Biogeosciences Discuss., doi:10.5194/bg-2016-282, 2016
Manuscript under review for journal Biogeosciences
Published: 11 July 2016

References

Aguilar-Islas, A. and Bruland, K.: Dissolved manganese and silicic acid in the Columbia River plume, Mar. Chem., 101, 233–247, doi:10.1016/j.marchem.2006.03.005, 2006.

Aumont, O., Ethé, C., Tagliabue, A., Bopp, L., and Gehlen, M.: PISCES-v2: an ocean biogeochemical model for carbon and ecosystem studies, Geosci. Model Dev., 8, 2465–2513, doi:10.5194/gmd-8-2465-2015, 2015.

Baker, A., Jickells, T., Witt, M., and Linge, K.: Trends in the solubility of iron, aluminium, manganese and phosphorus in aerosol collected over the Atlantic Ocean, Mar. Chem., 98, 43–58, doi:10.1016/j.marchem.2005.06.004, 2006.

Baker, A., Landing, W., Bucciarelli, E., Fietz, S., Hayes, C., Kadko, D., Morton, P., Rogan, N., Sarthou, G., Shelley, R., Shi, Z., Shiller, A., and Van Hulten, M.M.P.: Trace Element and Isotope Deposition across the Air – Sea Interface: Progress and Research Needs, Phil. Trans. R. Soc. A, doi:10.1098/not yet assigned, part of the special issue **?**., in preparation.

Balistrieri, L., Brewer, P., and Murray, J.: Scavenging residence times of trace metals and surface chemistry of sinking particles in the deep ocean, Deep-Sea Res. Pt A, 28, 101–121, 1981.

Balzer, W.: On the distribution of iron and manganese at the sediment/water interface: thermodynamic versus kinetic control, Geochim. Cosmochim. Ac., 46, 1153–1161, doi:10.1016/0016-7037(82)90001-1, 1982.

Barnier, B., Madec, G., Penduff, T., Molines, J.-M., Tréguier, A.-M., Sommer, J. l., Beckmann, A., Biastoch, A., Böning, C., Dengg, J., Derval, C., Durand, E., Gulev, S., Remy, E., Talandier, C., Theetten, S., Maltrud, M., McClean, J., and Cuevas, B. D.: Impact of partial steps and momentum advection schemes in a global ocean circulation model at eddy-permitting resolution, Ocean Dynamics, 56, 543–567, doi:10.1007/s10236-006-0082-1, http://archimer.ifremer.fr/doc/2006/publication-3514.pdf, 2006.

Bender, M. L., Klinkhammer, G. P., and Spencer, D. W.: Manganese in seawater and the marine manganese balance, Deep-Sea Res., 24, 799–812, doi:10.1016/0146-6291(77)90473-8, 1977.

Bishop, J. K. and Fleisher, M. Q.: Particulate manganese dynamics in Gulf Stream warm-core rings and surrounding waters of the N.W. Atlantic, Geochim. Cosmochim. Ac., 51, 2807–2825, doi:10.1016/0016-7037(87)90160-8, 1987.

Bortleson, G. and Lee, G.: Phosphorus, iron, and manganese distribution in sediment cores of six Wisconsin lakes, Limnol. Oceanogr., 19, 794–801, 1974.

Bowers, T., Campbell, A., Measures, C., Spivack, A., Khadem, M., and Edmond, J.: Chemical controls on the composition of vent fluids at 13°–11° N and 21° N, East Pacific Rise, J. Geophys. Res., 93, 4522–4536, doi:10.1029/JB093iB05p04522, 1988.

Boye, M., Wake, B. D., Garcia, P. L., Bown, J., Baker, A. R., and Achterberg, E. P.: Distributions of dissolved trace metals (Cd, Cu, Mn, Pb, Ag) in the southeastern Atlantic and the Southern Ocean, Biogeosci., 9, 3231–3246, doi:10.5194/bg-9-3231-2012, 2012.

Boyle, E. A., Bergquist, B. A., Kayser, R. A., and Mahowald, N.: Iron, manganese, and lead at Hawaii Ocean Time-series station ALOHA, Geochim. Cosmochim. Ac., 69, 933–952, doi:10.1016/j.gca.2004.07.034, 2005.

Browning, T. J., Bouman, H. A., Henderson, G. M., Mather, T. A., Pyle, D. M., Schlosser, C., Woodward, E. M. S., and Moore, C. M.: Strong responses of Southern Ocean phytoplankton communities to volcanic ash, Geophys. Res. Lett., 41, 2851–2857, doi:10.1002/2014GL059364, 2014.

Bruland, K. and Lohan, M.: Controls of Trace Metals in Seawater, in: The Oceans and Marine Geochemistry, edited by Elderfield, H., vol. 6, chap. 6.02, pp. 23–47, Elsevier, http://es.ucsc.edu/~kbruland/Manuscripts/BRULAND/BrulandChpt6_02_TraceMetals.pdf, 2006.

Bruland, K., Orians, K., and J.P., C.: Reactive trace metals in the stratified central North Pacific, Geochim. Cosmochim. Ac., 58, 3171–3182, doi:10.1016/0016-7037(94)90044-2, 1994.

Biogeosciences Discuss., doi:10.5194/bg-2016-282, 2016
Manuscript under review for journal Biogeosciences
Published: 11 July 2016

Buck, C., Landing, W., Resing, J., and Measures, C.: The solubility and deposition of aerosol Fe and other trace elements in the North Atlantic Ocean, Mar. Chem., 120, 57–70, doi:10.1016/j.marchem.2008.08.003, 2010.

Buma, A. G. J., de Baar, H. J. W., Nolting, R. F., and van Bennekom, A. J.: Metal enrichment experiments in the Weddell-Scotia Seas: Effects of iron and manganese on various plankton communities, Limnol. Oceanogr., 36, 1865–1878, doi:10.4319/lo.1991.36.8.1865, 1991.

Charette, M., Lam, P., Lohan, M., Kwon, E., Hatjee, V., Jeandel, C., Shillerg, A., Cutterh, G., Thomas, A., Boyd, P., Homoky, W., Milne, A., Thomas, H., Andersson, P., Porcellio, D., Tanakap, T., Geibert, W., Dehairs, F., and Gardia-Orellana, J.: Coastal ocean and shelf-sea biogeochemical cycling of trace elements and isotopes: lessons learned from GEOTRACES, Phil. Trans. R. Soc. A, doi:10.1098/not yet assigned, part of the special issue **?**., in preparation.

Coale, K. H.: Effects of iron, manganese, copper, and zinc enrichments on productivity and biomass in the subarctic Pacific, Limnol. Oceanogr., 36, 1851–1864, doi:10.4319/lo.1991.36.8.1851, 1991.

Corliss, J. and Dymond, J.: on the Galapagos Rift, Science, 203, 16, doi:10.1126/science.203.4385.1073, 1979.

Doi, T., Obata, H., and Maruo, M.: Shipboard analysis of picomolar levels of manganese in seawater by chelating resin concentration and chemiluminescence detection, Anal. Bioanal. Chem., 378, 1288–1293, doi:10.1007/s00216-003-2483-z, 2004.

Douville, E., Charlou, J., Oelkers, E., Bienvenu, P., Jove Colon, C., Donval, J., Fouquet, Y., Prieur, D., and Appriou, P.: The rainbow vent fluids (36°14' N, MAR), Chemical Geology, 184, 37–48, doi:10.1016/S0009-2541(01)00351-5, 2002.

Dutay, J., Jean-Baptiste, P., Campin, J., Ishida, A., Maier-Reimer, E., Matear, R., Mouchet, A., Totterdell, I., Yamanaka, Y., Rodgers, K., et al.: Evaluation of OCMIP-2 ocean models' deep circulation with mantle helium-3, J. Mar. Syst., 48, 15–36, doi:10.1016/j.jmarsys.2003.05.010, 2004.

De Baar, H.J.W., Timmermans, K., Laan, P., De Porto, H., Ober, S., Blom, J., Bakker, M., Schilling, J., Sarthou, G., Smit, M., et al.: Titan: A new facility for ultraclean sampling of trace elements and isotopes in the deep oceans in the international Geotraces program, Mar. Chem., 111, 4–21, doi:10.1016/j.marchem.2007.07.009, 2008.

Von Langen, P.J., Johnson, K., Coale, K., and Elrod, V.: Oxidation kinetics of manganese (II) in seawater at nanomolar concentrations, Geochim. Cosmochim. Ac., 61, 4945–4954, doi:10.1016/S0016-7037(97)00355-4, 1997.

Elderfield, H.: Manganese fluxes to the oceans, Mar. Chem., 4, 103–132, 1976.

Fraústo da Silva, J. and Williams, R.: The biological chemistry of the elements: the inorganic chemistry of life, Oxford University Press, 2 edn., 2001.

Froelich, P., Klinkhammer, G., Bender, M., Luedtke, N., Heath, G., Cullen, D., Dauphin, P., Hammond, D., Hartman, B., and Maynard, V.: Early oxidation of organic matter in pelagic sediments of the eastern equatorial Atlantic: suboxic diagenesis, Geochim. Cosmochim. Ac., 43, 1075–1090, doi:10.1016/0016-7037(79)90095-4, 1979.

Gaspar, P., Gregoris, Y., and Lefevre, J. M.: A simple eddy kinetic energy model for simulations of the ocean vertical mixing: Tests at station Papa and Long-Term Upper Ocean Study Site site, J. Geophys. Res., 95, 16,179–16,193, doi:10.1029/JC095iC09p16179, 1990.

Gent, P. and McWilliams, J.: Isopycnal mixing in ocean circulation models, J. Phys. Oceanogr., 20, 150–155, doi:10.1175/1520-0485(1990)020<0150:IMIOCM>2.0.CO;2, 1990.

German, C., Casciotti, K., Dutay, J.-C., Heimbürger, L., Jenkins, W., Measures, C., Mills, R., Obata, H., Schlitzer, R., Tagliabue, A., Turner, D., and Whitby, H.: Hydrothermal Impacts on Trace Element and Isotope Ocean Biogeochemistry, Phil. Trans. R. Soc. A, doi:10.1098/not yet assigned, part of the special issue *Biological and climatic impacts of ocean trace element chemistry*, in preparation.

Guieu, C., Duce, R., and Arimoto, R.: Dissolved input of manganese to the ocean: Aerosol source, J. Geophys. Res. Atmos., 99, 18 789–18, doi:10.1029/94JD01120, 1994.

Biogeosciences Discuss., doi:10.5194/bg-2016-282, 2016
Manuscript under review for journal Biogeosciences
Published: 11 July 2016

Hauglustaine, D., Hourdin, F., Jourdain, L., Filiberti, M.-A., Walters, S., Lamarque, J.-F., and Holland, E.: Interactive chemistry in the Laboratoire de Météorologie Dynamique general circulation model, J. Geophys. Res.: Atmospheres, 109, D04 314, doi:10.1029/2003JD003957, 2004.

Hayes, C. T., Anderson, R. F., Fleisher, M. Q., Lam, P. J., Ohnemus, D. C., Huang, K.-F., Robinson, L. F., Lu, Y., Cheng, H., Edwards, R. L., and Moran, S. B.: Intensity of Th and Pa scavenging partitioned by particle chemistry in the North Atlantic Ocean, Mar. Chem., doi:10.1016/j.marchem.2015.01.006, 2015.

Homoky, W., Weber, T., Berelson, W., Conway, T., Henderson, G., Van Hulten, M.M.P., Jeandel, C., Severmann, S., and Tagliabue, A.: An assessment of oceanic trace element and isotope fluxes at the sediment-water boundary, Phil. Trans. R. Soc. A, doi:10.1098/not yet assigned, part of the special issue **?**., in preparation.

Van Hulten, M.M.P.: Aluminium and Manganese in the West Atlantic Ocean, Ph.D. thesis, University of Groningen, http://irs.ub.rug.nl/ppn/384091636, printed version available on request to the author, 2014.

Van Hulten, M.M.P., Sterl, A., Dutay, J.-C., Tagliabue, A., Gehlen, M., De Baar, H.J.W., and Middag, R.: Aluminium in an ocean general circulation model compared with the West Atlantic Geotraces cruises, J. Mar. Syst., 126, 3–23, doi:10.1016/j.jmarsys.2012.05.005, traces and Tracers: Selected papers from the Joint Liège Colloquium on Ocean Dynamics – Bonus-GoodHope – Geotraces meeting, 2013.

Van Hulten, M.M.P., Sterl, A., Middag, R., de Baar, H., Gehlen, M., Dutay, J.-C., and Tagliabue, A.: On the effects of circulation, sediment resuspension and biological incorporation by diatoms in an ocean model of aluminium, Biogeosci., 11, 3757–3779, doi:10.5194/bg-11-3757-2014, 2014.

Hydes, D., Statham, P., and Burton, J.: A vertical profile of dissolved trace metals (Al, Cd, Cu, Mn, Ni) over the median valley of the mid Atlantic ridge, 43° N, Sci. Total Environ., 49, 133–145, doi:10.1016/0048-9697(86)90236-6, 1986.

Jeandel, C.: Introduction mechanisms that could explain the "Boundary Exchange" at the land–ocean contact, Phil. Trans. R. Soc. A, doi:10.1098/not yet assigned, part of the special issue **?**., in preparation.

Jeandel, C., van der Loeff, M. R., Lam, P. J., Roy-Barman, M., Sherrell, R. M., Kretschmer, S., German, C., and Dehairs, F.: What did we learn about ocean particle dynamics in the GEOSECS–JGOFS era?, Progress in Oceanography, 133, 6–16, doi:10.1016/j.pocean.2014.12.018, GEOTRACES Synthesis and Modeling: The role of particles in the marine biogeochemical cycles of trace elements and their isotopes, 2015.

Jickells, T.: Atmospheric inputs of metals and nutrients to the oceans, Mar. Chem., 48, 199–214, doi:10.1016/0304-4203(95)92784-P, 1995.

Johnson, K., Coale, K., Berelson, W., and Michael Gordon, R.: On the formation of the manganese maximum in the oxygen minimum, Geochim. Cosmochim. Ac., 60, 1291–1299, doi:10.1016/0016-7037(96)00005-1, 1996.

Johnson, K., Elrod, V., Fitzwater, S., Plant, J., Boyle, E., Bergquist, B., Bruland, K., Aguilar-Islas, A., Buck, K., Lohan, M., et al.: Developing standards for dissolved iron in seawater, Eos, Transactions American Geophysical Union, 88, 131–132, doi:10.1029/2007EO110003, 2007.

De Jong, J., Boyé, M., Gelado-Caballero, M., Timmermans, K., Veldhuis, M., Nolting, R., van den Berg, C., and de Baar, H.: Inputs of iron, manganese and aluminium to surface waters of the Northeast Atlantic Ocean and the European continental shelf, Mar. Chem., 107, 120–142, doi:10.1016/j.marchem.2007.05.007, 2007.

Kawagucci, S., Okamura, K., Kiyota, K., Tsunogai, U., Sano, Y., Tamaki, K., and Gamo, T.: Methane, manganese, and helium-3 in newly discovered hydrothermal plumes over the Central Indian Ridge, 18°–20° S, Geochemistry, Geophysics, Geosystems, 9, doi:10.1029/2008GC002082, 2008.

Biogeosciences Discuss., doi:10.5194/bg-2016-282, 2016
Manuscript under review for journal Biogeosciences
Published: 11 July 2016

Klinkhammer, G. and Bender, M.: The distribution of manganese in the Pacific Ocean, Earth Planet. Sc. Lett., 46, 361–384, doi:10.1016/0012-821X(80)90051-5, 1980.

Klinkhammer, G., Bender, M., and Weiss, R.: Hydrothermal manganese in the Galapagos Rift, Nature, 269, 319–320, doi:10.1038/269319a0, 1977.

Klinkhammer, G., Rona, P., Greaves, M., and Elderfield, H.: Hydrothermal manganese plumes in the Mid-Atlantic Ridge rift valley, Nature, 314, 727–731, doi:10.1038/314727a0, 1985.

Klinkhammer, G., Chin, C., Keller, R., Daehlmann, A., Sahling, H., Sarthou, G., Petersen, S., Smith, F., and Wilson, C.: Discovery of new hydrothermal vent sites in Bransfield Strait, Antarctica, Earth Planet. Sc. Lett., 193, 395–407, doi:10.1016/S0012-821X(01)00536-2, 2001.

Landing, W. and Bruland, K.: Manganese in the north Pacific, Earth Planet. Sc. Lett., 49, 45–56, doi:10.1016/0012-821X(80)90149-1, 1980.

Landing, W. and Bruland, K.: The contrasting biogeochemistry of iron and manganese in the Pacific Ocean, Geochim. Cosmochim. Ac., 51, 29–43, doi:10.1016/0016-7037(87)90004-4, 1987.

Landing, W., Haraldsson, C., and Paxeus, N.: Vinyl polymer agglomerate based transition metal cation-chelating ion-exchange resin containing the 8-hydroxyquinoline functional group, Anal. Chem., 58, 3031–3035, doi:10.1021/ac00127a029, 1986.

Landing, W., Cutter, G., Dalziel, J., Flegal, A., Powell, R., Schmidt, D., Shiller, A., Statham, P., Westerlund, S., and Resing, J.: Analytical intercomparison results from the 1990 Intergovernmental Oceanographic Commission open-ocean baseline survey for trace metals: Atlantic Ocean, Mar. Chem., 49, 253–265, 1995.

Lavelle, J. W., Cowen, J. P., and Massoth, G. J.: A model for the deposition of hydrothermal manganese near ridge crests, J. Geophys. Res.: Oceans, 97, 7413–7427, doi:10.1029/92JC00406, 1992.

Leggett, R. W. and Williams, L. R.: A reliability index for models, Ecological Modelling, 13, 303–312, doi:10.1016/0304-3800(81)90034-X, 1981.

Lengaigne, M., Madec, G., Menkes, C., and Alory, G.: Effect of isopycnal diffusion in the tropical Pacific Ocean, J. Geophys. Res., 108, 10.1029/2002JC001 704, doi:10.1029/2002JC001704, 2003.

Lewis, B. L. and Luther, G. W.: Processes controlling the distribution and cycling of manganese in the oxygen minimum zone of the Arabian Sea, Deep-Sea Res. Pt II, 47, 1541–1561, doi:10.1016/S0967-0645(99)00153-8, 2000.

Li, Y.-H., Bischoff, J., and Mathieu, G.: The migration of manganese in the Arctic basin sediment, Earth Planet. Sc. Lett., 7, 265–270, doi:10.1016/0012-821X(69)90063-6, 1969.

Madec, G.: NEMO ocean engine, Note du Pole de Modélisation, Institut Pierre-Simon Laplace, 2008.

Madec, G., Delecluse, P., Imbard, M., and Lévy, C.: OPA 8.1 Ocean General Circulation Model reference manual, Note du Pole de Modélisation, Institut Pierre-Simon Laplace, 11, 91p, http://hal.archives-ouvertes.fr/hal-00154217/en/, 1998.

Madison, A., Tebo, B., Mucci, A., Sundby, B., and Luther, G.: Abundant Porewater Mn(III) Is a Major Component of the Sedimentary Redox System, Science, 341, 875–878, doi:10.1126/science.1241396, 2013.

Martin, J. and Knauer, G.: VERTEX, Deep-Sea Res. Pt A, 30, 411–425, 1983.

Mawji, E., Schlitzer, R., Dodas, E. M., Abadie, C., Abouchami, W., Anderson, R. F., Baars, O., Bakker, K., Baskaran, M., Bates, N. R., Bluhm, K., Bowie, A., Bown, J., Boye, M., Boyle, E. A., Branellec, P., Bruland, K. W., Brzezinski, M. A., Bucciarelli, E., Buesseler, K., Butler, E., Cai, P., Cardinal, D., Casciotti, K., Chaves, J., Cheng, H., Chever, F., Church, T. M., Colman, A. S., Conway, T. M., Croot, P. L., Cutter, G. A., de Baar, H. J., de Souza, G. F., Dehairs, F., Deng, F., Dieu, H. T., Dulaquais, G., Echegoyen-Sanz, Y., Edwards, R. L., Fahrbach, E., Fitzsimmons, J., Fleisher, M., Frank, M., Friedrich, J., Fripiat, F., Galer, S. J., Gamo, T., Solsona, E. G., Gerringa, L. J., Godoy, J. M., Gonzalez, S., Grossteffan, E., Hatta, M., Hayes, C. T., Heller, M. I., Henderson, G., Huang, K.-F., Jeandel, C., Jenkins,

W. J., John, S., Kenna, T. C., Klunder, M., Kretschmer, S., Kumamoto, Y., Laan, P., Labatut, M., Lacan, F., Lam, P. J., Lannuzel, D., le Moigne, F., Lechtenfeld, O. J., Lohan, M. C., Lu, Y., Masqué, P., McClain, C. R., Measures, C., Middag, R., Moffett, J., Navidad, A., Nishioka, J., Noble, A., Obata, H., Ohnemus, D. C., Owens, S., Planchon, F., Pradoux, C., Puigcorbé, V., Quay, P., Radic, A., Rehkämper, M., Remenyi, T., Rijkenberg, M. J., Rintoul, S., Robinson, L. F., Roeske, T., Rosenberg, M., van der Loeff, M. R., Ryabenko, E., Saito, M. A., Roshan, S., Salt, L., Sarthou, G., Schauer, U., Scott, P., Sedwick, P. N., Sha, L., Shiller, A. M., Sigman, D. M., Smethie, W., Smith, G. J., Sohrin, Y., Speich, S., Stichel, T., Stutsman, J., Swift, J. H., Tagliabue, A., Thomas, A., Tsunogai, U., Twining, B. S., van Aken, H. M., van Heuven, S., van Ooijen, J., van Weerlee, E., Venchiarutti, C., Voelker, A. H., Wake, B., Warner, M. J., Woodward, E. M. S., Wu, J., Wyatt, N., Yoshikawa, H., Zheng, X.-Y., Xue, Z., Zieringer, M., and Zimmer, L. A.: The GEOTRACES Intermediate Data Product 2014, Mar. Chem., 177, doi:10.1016/j.marchem.2015.04.005, 2015.

McCave, I.: Vertical flux of particles in the ocean, Deep-Sea Res. and Oceanographic Abstracts, 22, 491–502, doi:10.1016/0011-7471(75)90022-4, 1975.

McManus, J., Berelson, W. M., Severmann, S., Johnson, K. S., Hammond, D. E., Roy, M., and Coale, K. H.: Benthic manganese fluxes along the Oregon–California continental shelf and slope, Cont. Shelf Res., 43, 71–85, doi:10.1016/j.csr.2012.04.016, 2012.

Means, J. L., Crerar, D. A., Borcsik, M. P., and Duguid, J. O.: Radionuclide adsorption by manganese oxides and implications for radioactive waste disposal, Nature, 274, 44–47, doi:10.1038/274044a0, 1978.

Mendez, J., Guieu, C., and Adkins, J.: Atmospheric input of manganese and iron to the ocean: Seawater dissolution experiments with Saharan and North American dusts, Mar. Chem., 120, 34–43, doi:10.1016/j.marchem.2008.08.006, 2010.

Middag, R.: Dissolved Aluminium and Manganese in the Polar Oceans, Ph.D. thesis, University of Groningen, 2010.

Middag, R., de Baar, H., Laan, P., and Bakker, K.: Dissolved aluminium and the silicon cycle in the Arctic Ocean, Mar. Chem., 115, 176–195, doi:10.1016/j.marchem.2009.08.002, 2009.

Middag, R., de Baar, H., Laan, P., Cai, P., and van Ooijen, J.: Dissolved manganese in the Atlantic sector of the Southern Ocean, Deep-Sea Res. Pt II, 58, 2661–2677, doi:10.1016/j.dsr2.2010.10.043, 2011a.

Middag, R., de Baar, H., Laan, P., and Klunder, M.: Fluvial and hydrothermal input of manganese into the Arctic Ocean, Geochim. Cosmochim. Ac., 75, 2393–2408, doi:10.1016/j.gca.2011.02.011, 2011b.

Middag, R., de Baar, H., Laan, P., and Huhn, O.: The effects of continental margins and water mass circulation on the distribution of dissolved aluminum and manganese in Drake Passage, J. Geophys. Res., 117, C01 019, doi:10.1029/2011JC007434, 2012.

Middag, R., de Baar, H., Klunder, M., and Laan, P.: Fluxes of dissolved aluminum and manganese to the Weddell Sea and indications for manganese co-limitation, Limnol. Oceanogr., 58, 287–300, doi:10.4319/lo.2013.58.1.0287, 2013.

Middag, R., Van Hulten, M.M.P., Van Aken, H.M., Rijkenberg, M., Gerringa, L., Laan, P., and De Baar, H.J.W.: Dissolved aluminium in the ocean conveyor of the West Atlantic Ocean: Effects of the biological cycle, scavenging, sediment resuspension and hydrography, Mar. Chem., 177, Part 1, 69–86, doi:10.1016/j.marchem.2015.02.015, biogeochemistry of trace elements and their isotopes, 2015.

Middag, R. et al.: Dissolved manganese along the West Atlantic GA02 GEOTRACES transects (working title), http://neon.otago.ac.nz/chemistry/contacts/profile/rm, in preparation.

Middelburg, J. J., Soetaert, K., Herman, P. M. J., and Heip, C. H. R.: Denitrification in marine sediments: A model study, Global Biogeochem. Cy., 10, 661–673, doi:10.1029/96GB02562, 1996.

Milne, A. and Landing, W.: CLIVAR P16: Dissolved manganese in the upper 1000 m of the Pacific Ocean, unpublished data.

Biogeosciences Discuss., doi:10.5194/bg-2016-282, 2016
Manuscript under review for journal Biogeosciences
Published: 11 July 2016

Milne, A., Landing, W., Bizimis, M., and Morton, P.: Determination of Mn, Fe, Co, Ni, Cu, Zn, Cd and Pb in seawater using high resolution magnetic sector inductively coupled mass spectrometry (HR-ICP-MS), Analytica Chimica Acta, 665, 200–207, doi:10.1016/j.aca.2010.03.027, 2010.

Murray, J. W.: The interaction of metal ions at the manganese dioxide-solution interface, Geochim. Cosmochim. Ac., 39, 505–519, doi:10.1016/0016-7037(75)90103-9, 1975.

Nealson, K. H.: The Manganese-Oxidizing Bacteria, in: The Prokaryotes: Volume 5: Proteobacteria: Alpha and Beta Subclasses, edited by Dworkin, M., Falkow, S., Rosenberg, E., Schleifer, K.-H., and Stackebrandt, E., pp. 222–231, Springer New York, New York, NY, doi:10.1007/0-387-30745-1_11, 2006.

Noble, A. E., Lamborg, C. H., Ohnemus, D. C., Lam, P. J., Goepfert, T. J., Frame, C. H., Casciotti, K. L., DiTullio, G. R., Jennings, J. C., Saito, M. A., et al.: Basin-scale inputs of cobalt, iron, and manganese from the Benguela-Angola front to the South Atlantic Ocean, Limnol. Oceanogr., 2012.

Pakhomova, S., Hall, P., Kononets, M., Rozanov, A., Tengberg, A., and Vershinin, A.: Fluxes of iron and manganese across the sediment–water interface under various redox conditions, Mar. Chem., 107, 319–331, doi:10.1016/j.marchem.2007.06.001, 2007.

Passow, U. and De La Rocha, C. L.: Accumulation of mineral ballast on organic aggregates, Global Biogeochem. Cy., 20, doi:10.1029/2005GB002579, 2006.

Peers, G. and Price, N.: A Role for Managanese in Superoxide Dismutases and Growth of Iron-Deficient Diatoms, Limnol. Oceanogr., 49, 1774–1783, doi:10.4319/lo.2004.49.5.1774, 2004.

Raven, J. A.: Predictions of Mn and Fe use efficiencies of phototrophic growth as a function of light availability for growth and of C assimilation pathway, New Phytologist, 116, 1–18, doi:10.1111/j.1469-8137.1990.tb00505.x, 1990.

Reid, D. F., Key, R. M., and Schink, D. R.: Radium, thorium, and actinium extraction from seawater using an improved manganese-oxide-coated fiber, Earth Planet. Sc. Lett., 43, 223–226, doi:10.1016/0012-821X(79)90205-X, 1979.

Resing, J. A., Sedwick, P. N., German, C. R., Jenkins, W. J., Moffett, J. W., Sohst, B. M., and Tagliabue, A.: Basin-scale transport of hydrothermal dissolved metals across the South Pacific Ocean, Nature, 523, 200–203, doi:10.1038/nature14577, 2015.

Rijkenberg, M. J., de Baar, H. J., Bakker, K., Gerringa, L. J., Keijzer, E., Laan, M., Laan, P., Middag, R., Ober, S., van Ooijen, J., Ossebaar, S., van Weerlee, E. M., and Smit, M. G.: "PRISTINE", a new high volume sampler for ultraclean sampling of trace metals and isotopes, Mar. Chem., 177, Part 3, 501–509, doi:10.1016/j.marchem.2015.07.001, cycles of metals and carbon in the oceans–A tribute to the work stimulated by Hein de Baar, 2015.

Roy-Barman, M.: Modelling the effect of boundary scavenging on Thorium and Protactinium profiles in the ocean, Biogeosci., 6, 3091–3107, doi:10.5194/bg-6-3091-2009, 2009.

Roy-Barman, M., Jeandel, C., Souhaut, M., Rutgers van der Loeff, M., Voege, I., Leblond, N., and Freydier, R.: The influence of particle composition on thorium scavenging in the NE Atlantic ocean (POMME experiment), Earth Planet. Sc. Lett., 240, 681–693, doi:10.1016/j.epsl.2005.09.059, 2005.

Rüth, C., Well, R., and Roether, W.: Primordial ^{3}He in South Atlantic deep waters from sources on the Mid-Atlantic Ridge, Deep-Sea Res. Pt I, 47, 1059–1075, doi:10.1016/S0967-0637(99)00077-1, 2000.

Saager, P. M., de Baar, H. J., and Burkill, P. H.: Manganese and iron in Indian Ocean waters, Geochim. Cosmochim. Ac., 53, 2259–2267, doi:10.1016/0016-7037(89)90348-7, 1989.

Saito, M. A., Moffett, J. W., and DiTullio, G. R.: Cobalt and nickel in the Peru upwelling region: A major flux of labile cobalt utilized as a micronutrient, Global Biogeochem. Cy., 18, doi:10.1029/2003GB002216, 2004.

Biogeosciences Discuss., doi:10.5194/bg-2016-282, 2016
Manuscript under review for journal Biogeosciences
Published: 11 July 2016

Sander, S. and Koschinsky, A.: Metal flux from hydrothermal vents increased by organic complexation, Nat. Geosci., 4, 145–150, doi:10.1038/ngeo1088, 2011.

Sarmiento, J. and Gruber, N.: Ocean Biogeochemical Dynamics, Princeton University Press, 2006.

Slemons, L., Murray, J., Resing, J., Paul, B., and Dutrieux, P.: Western Pacific coastal sources of iron, manganese, and aluminum to the Equatorial Undercurrent, Global Biogeochem. Cy., 24, doi:10.1029/2009GB003693, 2010.

Slomp, C., Malschaert, J., Lohse, L., and Van Raaphorst, W.: Iron and manganese cycling in different sedimentary environments on the North Sea continental margin, Cont. Shelf Res., 17, 1083–1117, doi:10.1016/S0278-4343(97)00005-8, 1997.

Statham, P., Yeats, P., and Landing, W.: Manganese in the eastern Atlantic Ocean, Mar. Chem., 61, 55–68, 1998.

Stone, A. and Morgan, J.: Kinetics of Chemical Transformation in the Environment, in: Aquatic chemical kinetics, edited by Stumm, W., vol. 2, chap. 1, pp. 1–42, John Wiley and Sons, 1990.

Stow, C., Jolliff, J., Jr., D. M., Doney, S., Allen, J., Friedrichs, M., Rose, K., and Wallhead, P.: Skill assessment for coupled biological/physical models of marine systems, J. Mar. Syst., 76, 4–15, doi:10.1016/j.jmarsys.2008.03.011, 2009.

Sunda, W. and Huntsman, S.: Effect of sunlight on redox cycles of manganese in the southwestern Sargasso Sea, Deep-Sea Res. Pt A, 35, 1297–1317, doi:10.1016/0198-0149(88)90084-2, 1988.

Sunda, W. and Huntsman, S.: Photoreduction of manganese oxides in seawater, Mar. Chem., 46, 133–152, doi:10.1016/0304-4203(94)90051-5, 1994.

Sundby, B. and Silverberg, N.: Manganese fluxes in the benthic boundary layer, Limnol. Oceanogr., pp. 372–381, 1985.

Sundby, B., Silverberg, N., and Chesselet, R.: Pathways of manganese in an open estuarine system, Geochim. Cosmochim. Ac., 45, 293–307, doi:10.1016/0016-7037(81)90240-4, 1981.

Tagliabue, A., Bopp, L., Dutay, J.-C., Bowie, A., Chever, F., Jean-Baptiste, P., Bucciarelli, E., Lannuzel, D., Remenyi, T., Sarthou, G., Aumont, O., Gehlen, M., and Jeandel, C.: Hydrothermal contribution to the oceanic dissolved iron inventory, Nat. Geosci., 3, 252–256, doi:10.1038/NGEO818, 2010.

Tebo, B., Johnson, H., McCarthy, J., and Templeton, A.: Geomicrobiology of manganese (II) oxidation, Trends in Microbiology, 13, 421–428, doi:10.1016/j.tim.2005.07.009, 2005.

Thi Dieu Vu, H. and Sohrin, Y.: Diverse stoichiometry of dissolved trace metals in the Indian Ocean, Sci. Rep., 3, doi:10.1038/srep01745, 2013.

Tonkin, J. W., Balistrieri, L. S., and Murray, J. W.: Modeling sorption of divalent metal cations on hydrous manganese oxide using the diffuse double layer model, Applied Geochemistry, 19, 29–53, doi:10.1016/S0883-2927(03)00115-X, 2004.

Trefry, J. H. and Presley, B. J.: Manganese fluxes from Mississippi Delta sediments, Geochim. Cosmochim. Ac., 46, 1715–1726, doi:10.1016/0016-7037(82)90112-0, 1982.

Vichi, M. and Masina, S.: Skill assessment of the PELAGOS global ocean biogeochemistry model over the period 1980–2000, Biogeosci., 6, 2333–2353, doi:10.5194/bg-6-2333-2009, 2009.

Wedepohl, K.: The composition of the continental crust, Geochim. Cosmochim. Ac., 59, 1217–1232, doi:10.1016/0016-7037(95)00038-2, 1995.

Wu, J., Roshan, S., and Chen, G.: The distribution of dissolved manganese in the tropical-subtropical North Atlantic during US GEOTRACES 2010 and 2011 cruises, Mar. Chem., doi:10.1016/j.marchem.2014.08.007, 2014.

Yamagata, N. and Iwashima, K.: Monitoring of Sea-Water for Important Radioisotopes Released by Nuclear Reactors, Nature, 200, 52–52, doi:10.1038/200052a0, 1963.

Biogeosciences Discuss., doi:10.5194/bg-2016-282, 2016
Manuscript under review for journal Biogeosciences
Published: 11 July 2016

Yeats, P., Sundby, B., and Bewers, J.: Manganese recycling in coastal waters, Mar. Chem., 8, 43–55, doi:10.1016/0304-4203(79)90031-8, 1979.